



VALIDATION OF DRAFT
INTERNATIONAL
ELECTROTECHNICAL
COMMISSION 61853-2
STANDARD:
ANGLE OF INCIDENCE
EFFECT ON PHOTOVOLTAIC
MODULES

Prepared by:

Brett Knisely
Suryanarayana Vasantha Janakeeraman
Joseph Kuitche
Govindasamy TamizhMani

Arizona State University
Photovoltaic Reliability Laboratory

March 2013

Solar America Board for Codes and Standards

www.solarabcs.org



DISCLAIMER

This report was prepared as an account of work sponsored by an agency of the United States government. Neither the United States government nor any agency thereof, nor any of their employees, makes any warranty, express or implied, or assumes any legal liability or responsibility for the accuracy, completeness, or usefulness of any information, apparatus, product, or process disclosed, or represents that its use would not infringe privately owned rights. Reference herein to any specific commercial product, process, or service by trade name, trademark, manufacturer, or otherwise does not necessarily constitute or imply its endorsement, recommendation, or favoring by the United States government or any agency thereof. The views and opinions of authors expressed herein do not necessarily state or reflect those of the United States government or any agency thereof.

Download a copy of the report:

www.solarabcs.org/aoi

EXECUTIVE SUMMARY

The purpose of this study is to test and validate the draft International Electrotechnical Commission (IEC) 61853-2 standard's (IEC, 2012) experimental procedures and related mathematical models for the measurement of angle of incidence (AOI) effects on photovoltaic (PV) modules. This is a continuation of a previous project to test and validate the IEC 61853-1 standard. A comprehensive report related to the validation of the IEC 61853-1 standard can be downloaded from the Solar America Board for Codes and Standards (*Solar ABCs*) website (*Photovoltaic Module Power Rating per IEC 61853-1 Standard: A Study Under Natural Sunlight*, March 2011). Both of these experimental projects were carried out at Arizona State University Photovoltaic Reliability Laboratory according to the outdoor test procedure of the standard.

This validation study is important because PV modules are typically tested and rated only at three different test conditions—standard test conditions (STC) (1,000 watts per square meter [W/m^2] irradiance, 25°C cell temperature), low irradiance (200 W/m^2 irradiance, 25°C cell temperature), and nominal operating cell temperature (800 W/m^2 irradiance, 20°C ambient temperature). In addition, all these measurements are currently conducted at only a single spectral level of air mass 1.5 and at a single incidence angle of zero degree.

Installed modules, however, operate at a wide range of temperatures, irradiance levels, angles of incidence, and solar spectra. To accurately predict the energy production of the modules under various field conditions, it is necessary to characterize the modules at a wide range of temperatures, irradiances, angles of incidence, and spectra.

Toward that end, the IEC is developing the IEC 61853 standard titled “Photovoltaic Modules Performance Testing and Energy Rating.” This standard has four parts, and this Solar ABCs report focuses on the section of the second part (IEC 61853-2) concerned with AOI effects on PV modules. A working group of IEC Technical Group 82 developed the procedures and mathematical models used in the first two parts of the standard, and the accuracy of these procedures and models must be independently tested and validated. The IEC 61853-2 standard is in the IEC review and approval process and is expected to be released in 2015.

This report presents the effects of AOI on short circuit current (I_{sc}) for five different module technologies:

- monocrystalline silicon (mono-Si),
- polycrystalline silicon (poly-Si),
- amorphous silicon (a-Si),
- cadmium telluride (CdTe), and
- copper indium gallium selenide (CIGS).

The superstrate/encapsulant/substrate materials of each of these modules are:

- glass/ethylene vinyl acetate (EVA)/polymer—mono-Si,
- glass/EVA/polymer—poly-Si,
- glass/EVA/glass—a-Si,
- glass/EVA/glass—CdTe, and
- glass/EVA/polymer—CIGS.

In addition, we used:

- four irradiance sensors—Kipp & Zonen pyranometer, Eppley PSP pyranometer, Kipp & Zonen pyrliometer, and polycrystalline silicon reference cell—to measure global and direct irradiance levels,
- thermal sensors to measure the ambient temperature as well as the test module and reference cell temperatures,
- a data acquisition system to collect and store the output of thermal sensors and the I_{sc} of the test modules and reference cell, and
- an attitude reference heading device to directly measure AOI.

We conducted three rounds of measurements and improved the experimental setup and data processing strategies after each round based on lessons learned:

- During the first round (see Appendix C for details), we encountered
 - multi-curve tracer that could record and store data in one-minute intervals, which we determined was not fast enough for our purposes;
 - irradiance sensors that had not been calibrated, so that we could not confirm the accuracy of the measurements or calculate uncertainty; and
 - a human error in constructing Equation A6.
- During the second round (see Appendix D for details), we
 - used transducers and a data logger and multiplexer rather than a multi-curve tracer, which increased the data storage and measurement speed from one minute to 30 seconds;
 - identified and corrected the human error in Equation A6; and
 - found that the reference devices had still not been calibrated and we could not calculate the uncertainty analysis.
- During the third and final round of measurements (detailed in the body of this report), we incorporated the lessons learned from the first two rounds and used calibrated reference devices.

During the rotation of the tracker platform, the test equipment measured and stored I_{sc} and temperature of all the test modules, irradiance data from all the irradiance sensors, and AOI data from the attitude reference heading device. We processed the data according to the IEC 61853-2 model to determine the relative light transmission or relative optical response of all the test modules, free from the influence of the diffuse light component and the cosine effect. We also compared this data with the data derived for the air-glass interface using various theoretical light transmission models and with the data derived specifically for PV modules with glass superstrate using an empirical model developed by Sandia National Laboratories.

The major conclusions resulting from this project are:

- Accurate test results require meticulous experimental setup and rigorous test procedures.
- Test results show nearly identical relative light transmission plots for all five test modules with glass superstrate regardless of the type of PV cell technology (mono-Si, poly-Si, a-Si, CdTe, or CIGS). This indicates that the reflective losses are governed almost exclusively by the air-glass interface of the PV modules.

- The relative light transmission plots obtained using the IEC 61853-2 model were in good agreement with the plots obtained using the theoretical air-glass interface models and the empirical model developed by Sandia National Laboratories for the glass superstrate PV modules.
- The standard states that “for the flat glass superstrate modules, the AOI test does not need to be performed, rather, the data of a flat glass air interface can be used.” The results obtained in the current study validate this statement.

AUTHOR BIOGRAPHIES

Brett Knisely and Suryanarayana Vasantha Janakeeraman are M.S. students at Arizona State University (ASU). Both are research assistants at the ASU Photovoltaic Reliability Laboratory (ASU-PRL) evaluating the performance of photovoltaic (PV) modules under various outdoor conditions.

Joseph Kuitche is a Ph.D. student at ASU and manager of ASU-PRL. He has taught undergraduate level courses at ASU and has published five papers related to statistical reliability prediction of PV modules and several papers related to the performance and qualification testing of PV modules.

Dr. (Mani) Govindasamy TamizhMani is the president of TUV Rheinland PTL (Photovoltaic Testing Laboratory) and a professor in the Department of Electronic Systems at ASU. Dr. Mani has been involved in research and development activities related to PV and fuel cells for more than 28 years, and PV module testing and certification activities for more than 13 years. He has been involved in test standard development activities since 1996. He has been teaching graduate level courses and has published more than 60 journal and conference papers. Email: manit@asu.edu.

SOLAR AMERICA BOARD FOR CODES AND STANDARDS

The Solar America Board for Codes and Standards (Solar ABCs) provides an effective venue for all solar stakeholders. A collaboration of experts formally gathers and prioritizes input from groups such as policy makers, manufacturers, installers, and large- and small-scale consumers to make balanced recommendations to codes and standards organizations for existing and new solar technologies. The U.S. Department of Energy funds Solar ABCs as part of its commitment to facilitate widespread adoption of safe, reliable, and cost-effective solar technologies.

ACKNOWLEDGMENTS

The authors gratefully acknowledge the support and comments received from David King (DK Solar Works; formerly Sandia National Laboratories), Bill Marion (National Renewable Energy Laboratory [NREL]), John Wohlgemuth (NREL), George Kelly (BP Solar), and Sarah Kurtz (NREL).

TABLE OF CONTENTS

Disclaimer	2
Executive Summary	3
Author Biographies.....	6
Solar ABCs	6
Acknowledgments	6
Introduction	8
Background	9
Scope and Purpose of IEC 61853-2 Standard	11
Outdoor Measurement Procedure of IEC 61853-2 Standard.....	12
Outdoor Measurement Procedure of ASU-PRL	14
Results and Discussion.....	19
Uncertainty Analysis	23
Conclusions.....	24
Acronyms	25
References.....	26
Scope of Appendices	27
Appendix A: Sandia Procedure to Determine Relative Optical Response.....	28
Appendix B: Crosschecking of Aoi Device Using a Manual Method.....	31
Appendix C: Lessons Learned 1: Round 1 Measurements Using a Multi-Curve Tracer .	33
Appendix D: Lessons Learned 2: Round 2 Measurements Using a Data Logger.....	35
Appendix E: Inter-Comparison and Crosschecking of Pyranometers.....	37
Appendix F: Measurement of f_2 (AOI) Versus AOI in the Opposite Direction.....	40

INTRODUCTION

The reflected and transmitted fractions of incident light determine the amount of sunlight that reaches photovoltaic (PV) solar cells. Module design influences the reflections of this light within the superstrate and encapsulant and at the air/superstrate, superstrate/encapsulant, and encapsulant/cell interfaces. It also influences transmittances through the superstrate and encapsulant. These reflections and transmittances are functions of the solar incidence angle. The surface roughness and antireflective coatings of superstrates heavily influence the incident angle effect.

The purpose of this study is to test and validate the draft International Electrotechnical Commission (IEC) 61853-2 standard's (IEC, 2012) experimental procedures and related mathematical models for the measurement of angle of incidence (AOI) effects on PV modules. This is a continuation of a previous project to test and validate the IEC 61853-1 standard. A comprehensive report related to the validation of the IEC 61853-1 standard can be downloaded from the Solar America Board for Codes and Standards (*Solar ABCs*) website (*Photovoltaic Module Power Rating per IEC 61853-1 Standard: A Study Under Natural Sunlight*, March 2011).

This validation study is important because PV modules are typically tested and rated only at three different test conditions—standard test conditions (STC) (1,000 watts per square meter [W/m^2] irradiance, 25°C cell temperature), low irradiance (200 W/m^2 irradiance, 25°C cell temperature), and nominal operating cell temperature (800 W/m^2 irradiance, 20°C ambient temperature). In addition, all these measurements are currently conducted at only a single spectral level of air mass (AM) 1.5 and at a single incidence angle of zero degree.

In actual installations, however, modules operate at a wide range of temperatures, irradiance levels, angles of incidence, and solar spectra. To accurately predict the energy production of the modules under various field conditions, it is necessary to characterize the modules at a wide range of temperatures, irradiances, angles of incidence, and spectra.

Toward that end, the IEC is developing the IEC 61853 standard titled “Photovoltaic Modules Performance Testing and Energy Rating” to characterize PV modules at a wide range of test conditions. This standard has four parts. The first (IEC 61853-1) was released in January 2011 and deals with the characterization of PV modules at 23 test conditions of irradiance and temperature but at a single angle of incidence (zero degree) and a single spectrum (AM1.5). The second (IEC 61853-2) is in the IEC review and approval process and is expected to be released in 2015. It addresses the wide range of angles of incidence and spectral effects. The third and fourth parts of the standard deal with energy rating calculations and reference conditions respectively, and are still under development. A working group of IEC Technical Group 82 developed the procedures and mathematical models used in the first two parts of the standard, and the accuracy of these procedures and models must be independently tested and validated.

BACKGROUND

There are two primary ways AOI influences the short circuit current (I_{sc}), and thus the power output, of PV modules. The first is a purely mechanical/geometrical effect due to the module's orientation with respect to the incident sunlight. It is often referred to as the "cosine effect." It states that the irradiance incident on the module decreases with increasing AOI and it is proportional to $\cos(\text{AOI})$. The second way AOI influences I_{sc} is related to the optical effects or surface characteristics of the module itself. PV manufacturers go to great lengths to improve the optical characteristics of modules by incorporating antireflective coatings, rolled or textured glass, or other methods.

This report presents the effects of AOI on I_{sc} for five different module technologies:

- monocrystalline silicon (mono-Si),
- polycrystalline silicon (poly-Si),
- amorphous silicon (a-Si),
- cadmium telluride (CdTe), and
- copper indium gallium selenide (CIGS).

The superstrate/encapsulant/substrate materials of each of these modules are:

- glass/ethylene vinyl acetate (EVA)/polymer—mono-Si,
- glass/EVA/polymer—poly-Si,
- glass/EVA/glass—a-Si,
- glass/EVA/glass—CdTe, and
- glass/EVA/polymer—CIGS.

We conducted three rounds of measurements on these modules and improved the experimental setup and data processing strategies based on lessons learned in each of the the first two rounds:

- During the first round (see Appendix C for details), we encountered
 - a multi-curve tracer that could record and store data in one-minute intervals, which we determined was not fast enough for our purposes;
 - irradiance sensors that had not been calibrated, so that we could not confirm the accuracy of the measurements or calculate uncertainty; and
 - a human error in constructing Equation A6.
- During the second round (see Appendix D for details), we
 - used transducers and a data logger and multiplexer rather than a multi-curve tracer, which increased the data storage and measurement speed from one minute to 30 seconds;
 - identified and corrected the human error in Equation A6; and
 - found that the reference devices had still not been calibrated, and we could not calculate the uncertainty analysis.
- During the third and final round of measurements (detailed in the body of this report), we incorporated the lessons learned from the first two rounds and used calibrated reference devices.

We made all measurements on clear sunny days using a two-axis tracker. We used a novel device to accurately measure the AOI and three conventional reference devices to measure the irradiance—a pyranometer and a polycrystalline silicon reference cell to measure global irradiance and a pyrliometer to measure direct normal irradiance.

To help the reader understand the intent and requirements of the standard, we present a synopsis of the scope, purpose, and measurement procedures of the IEC 61853-2 standard in this report. We also explain the sensitivity of test results to the experimental setup and the rigorous test procedures required to execute this project. In addition, we describe the lessons learned before the final measurements were made. We thoroughly analyzed and compared our experimental results with various empirical and theoretical models developed by various organizations including IEC and Sandia National Laboratories.

SCOPE AND PURPOSE OF IEC 61853-2 STANDARD

The scope of the IEC 61853 series of standards includes:

- test methods to map module performance over a wide range of temperature and irradiance conditions (part 1),
- test methods to determine incidence angle effects, module operating temperature, and spectral response (part 2),
- procedures for evaluating instantaneous and integrated power and energy results and an approach for providing a numerical rating for the results obtained in part 3 (part 3), and
- a definition of reference day irradiance and climatic profiles (part 4).

The purpose of part 2 of the IEC 61853 standard (IEC 61853-2) is to define procedures for measuring AOI effects, operating temperature, and spectral response on module performance. This Solar ABCs report deals only with the procedures and measurements related to AOI effects.

OUTDOOR MEASUREMENT PROCEDURE OF IEC 61853-2 STANDARD

The measurement procedure of the IEC 61853-2 standard for AOI effects is based on collecting the I_{sc} data of the test modules over a wide range of light incident angle. The required test apparatus, experimental setup, and measurement procedures are briefly presented below. For detailed and exact procedures, refer to the standard (IEC, 2012).

Test Apparatus

The standard identifies the use and technical requirements of test apparatus, including:

- irradiance sensors to measure the global and direct irradiance levels (reference cell for global irradiance and direct irradiance level using shadowing/collimating method as described in the “measurement procedure” below or a combination of pyranometer for global irradiance and pyrheliometer for direct normal irradiance),
- thermal sensors to measure the ambient temperature as well as the test module and reference cell temperatures,
- a data acquisition system (DAS) to collect and store the output of thermal sensors and the I_{sc} of the test modules and reference cell,
- a two-axis tracker to mount the test modules and change the incident angles on the test modules, and
- an AOI measuring device to determine the tilt angle to the sun and verify the coplanarity of test modules and irradiance sensors.

Test Setup

- Clean the front surfaces of the test modules.
- Mount the modules on the two-axis tracker racking system.
- Connect all the sensors and test modules to the DAS.

Measurement Procedure

- If the diffuse component does not exceed 10 % of the total irradiance, then directly measured I_{sc} at various angles of incidence, $I_{sc}(\theta)$, can be used to calculate the relative angular light transmission data, $\tau(\theta)$, as delineated below. If the diffuse component exceeds 10 % of the total irradiance, then the measured $I_{sc}(\theta)$ should be corrected before use in the calculation of $\tau(\theta)$. The $I_{sc}(\theta)$ correction depends on the type of irradiance sensor used (PV reference cell or pyranometer).
- If a PV reference cell device is used as an irradiance sensor, the diffuse light component should not exceed 10 % of the total irradiance during the $I_{sc}(\theta)$ measurement period. If the diffuse component exceeds 10 %, it can be subtracted after measuring the angular response with blocked direct light component or the diffuse component can be blocked to below 10 % by reducing the field of view of the diffuse component; for example, by collimating the incident light reaching the test module.
- If the pyranometer and pyrheliometer are used as irradiance sensors, the diffuse component visible to the module is:

$$G_{diff} = G_{tpoa} - G_{dni} \cos(\theta) \quad (1)$$

Where:

G_{diff} is global diffuse irradiance

G_{tpoa} is the total irradiance in the plane of the module, as measured by a pyranometer in the module plane

G_{dni} is direct normal irradiance as measured by the pyrheliometer

θ corresponds to the tilt angle between the module normal and the direct solar irradiance.

The I_{sc} induced by the direct incident light can be estimated in the presence of the diffuse light component to be:

$$I_{\text{sc}}(\theta) = I_{\text{sc_measured}}(\theta) (1 - G_{\text{diff}} / G_{\text{tpoa}}) \quad (2)$$

- Use the two-axis tracker to rotate the test module with respect to the normal solar irradiance. Vary the angle between module normal and sunlight between -80° and $+80^\circ$ in steps of maximum 10° . Do a minimum of nine different angles to span the angles from 0 to 80° .
- The relative angular light transmission (or relative angular optical response) into the module is given by:

$$\tau(\theta) = I_{\text{sc}}(\theta) / (\cos(\theta) I_{\text{sc}}(0)) \quad (3)$$

OUTDOOR MEASUREMENT PROCEDURE OF ASU-PRL

During the outdoor measurements at the Arizona State University Photovoltaic Reliability Laboratory (ASU-PRL), we closely followed the measurement procedures of the IEC 61853-2 standard. We present the test apparatus, experimental setup, and measurement procedures used in this work below.

Test Apparatus

- Test modules: We used test modules of five different technologies: mono-Si, poly-Si, a-Si, CdTe, and CIGS. In all the five modules, the superstrate was glass. The superstrate/encapsulant/substrate materials of these five modules are: glass/EVA/polymer (mono-Si); glass/EVA/polymer (poly-Si); glass/EVA/glass (a-Si); glass/EVA/glass (CdTe); and glass/EVA/polymer (CIGS).
- Irradiance sensors: We used a PV reference cell (poly-Si), two pyranometers from two vendors (Eppley PSP and Kipp & Zonen), and a pyr heliometer (Kipp & Zonen), and calibrated all the irradiance sensors. For the data analysis in this report, we processed only the data obtained using the pyranometers and pyr heliometer.
- Thermal sensors: We attached Omega T-type thermocouples to the center of the backsheet of each module using thermal tape. The manufacturer gives the accuracy for the thermocouples as $\pm 1^\circ\text{C}$ or 0.75% for temperatures above 0°C when temperature is expressed in $^\circ\text{C}$.
- DAS: We used CR Magnetics DC current transducers to measure the I_{sc} for each module (Figure 1A). The transducers were kept in an air-conditioned shed to maintain a constant operating temperature and to comply with the manufacturer rated accuracy of 1%. A linear relation is given between current passing through the transducer and the voltage output by the transducer. We used a Campbell Scientific CR1000 data logger to record and store all the simultaneously collected data, including module I_{sc} , module temperature, and irradiance. Because temperatures of the five modules also had to be recorded, we used a multiplexer to provide the necessary number of inputs (Figure 1B). The CR1000 was also kept inside a temperature-controlled shed to meet the manufacturer rated accuracy of 1%.



(A)



(B)

Figure 1. (A) DC current transducers; (B) CR 1000 DAS with a multiplexer.

- Two-axis tracker: We used a two-axis tracker to mount the test modules, irradiance sensors, and AOI measuring device. Ideally, the tracker should have full range of motion in both azimuth and elevation angles to achieve high angles of incidence for any time of day. The tracker used for this experiment was limited to 180° rotation about the azimuth angle and 65° of rotation about the elevation angle. High AOI could be achieved by starting the experiment at a certain time of day (around 2:30 pm for our setup) so that the tracker could use its full azimuth range. Because it was necessary to obtain E_{dni} (direct normal irradiance) measurements throughout the experiment, the pyrheliometer was allowed to track the sun using another manual or automatic 2-axis tracker.
- AOI measuring device: To determine the tilt angle to the sun for all modules and reference devices mounted on the two-axis tracker, we used a 3DM-GX3-25 miniature attitude heading reference system (Figure 2A) from MicroStrain (www.microstrain.com). It consists of a triaxial accelerometer, triaxial magnetometer, temperature sensors, and processor that run an algorithm to give static and dynamic orientation measurements with a manufacturer rated accuracy of $\pm 0.5^\circ$ static accuracy and a $\pm 0.2^\circ$ repeatability. To comply with the static accuracy of the device, the tracker stopped for six seconds at each AOI. This allowed for a stable AOI reading from the device. We used AOI software to calculate the position of the sun relative to the modules' orientation, therefore providing the AOI. We mounted the device on the surface of a plastic platform (Figure 2B) at the end of a plastic bar extending from the tracker and coplanar to the modules. AOI data was measured and recorded by a laptop that was kept outside of the shed. The tracker operator manually rotated the two-axis tracker while referring to the laptop with software that displayed the AOI of the tracker and thus of the modules and irradiance devices. The AOI data and data recorded by the Campbell Scientific CR1000 data logger were combined by synchronizing the laptop's clock to that of the data logger.



(A)

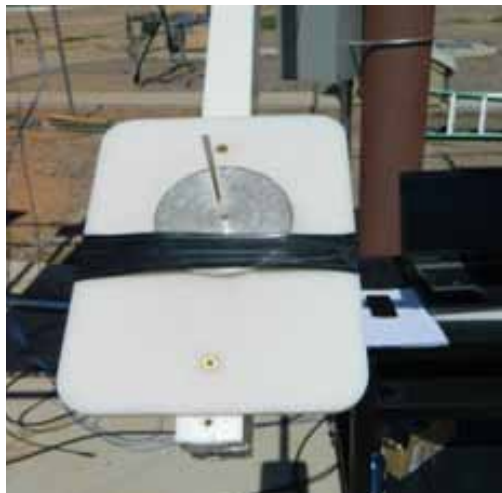
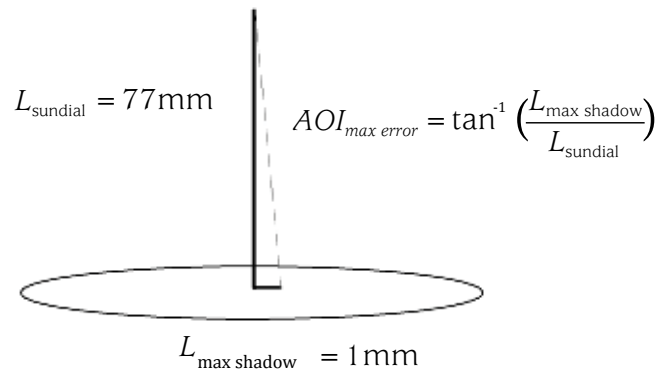


(B)

Figure 2. (A) AOI device; (B) AOI device mounted on a plastic arm.

Ideally, to ensure that all modules and reference devices are coplanar with respect to each other, the attitude heading reference device would be placed on each module and the AOI could be read from the software and checked for consistency. However, the accuracy of the device is greatly affected by any magnetic material. Although we were careful to ensure the device was mounted on a plastic platform with non-magnetic screws so that the measurement of AOI would not be affected, when

the 3DM-GX3-25 device is placed near the modules, an accurate reading of AOI is unobtainable. To check that all modules were coplanar with respect to each other, we set the tracker to automatic mode and allowed it to track at an angle normal to the solar incidence beam. We placed both the 3DM-GX3-25 device and a sundial on the plastic mounting arm of the AOI device and “zeroed” the tracker so that the AOI device measured a maximum AOI of 0.3° or less and there was no visible shadow on the sundial (Figure 3A). We then placed the sundial at the center and corner (Figure 3B) of each module and measured the shadow of the sundial for each location. As shown in the equation below, the point on the tracker with the longest shadow length represented the least accurate point with respect to AOI ($AOI_{max\ error}$). We measured this maximum shadow length and calculated the corresponding angle to be 0.7° . Given that the initial AOI reading was a maximum of 0.3° , the projected maximum uncertainty for AOI was $\pm 1.0^\circ$.



(A)

(B)

Figure 3. (A) Sundial “zeroed” to AOI platform with essentially no shadow present; (B) Using the sundial to check the accuracy of AOI for the mono-Si module.

Test Setup

Figure 4 shows the setup we used for this experiment. As required by the standard, we cleaned all the modules before beginning the measurements. In Figure 4, we include the name of each module technology next to the respective module, and identify all the components and test apparatus used in this work.



Figure 4. AOI measurement setup on a two-axis tracker.

Measurement Procedure

To reduce the effects of module temperature, solar irradiance, and solar spectral variations, the data should be collected as quickly as possible. For this experiment, data was simultaneously collected for five different modules and irradiance sensors. We paid careful attention to the following factors during the experiment:

1. **Soiling:** Dust on the surface of the modules can influence the irradiance incident on the surface of the module. Therefore, we cleaned all modules before each experiment.
2. **Reflection from the surroundings:** There should be no objects of abnormally high solar reflectance at the test sight. We were careful to prevent reflection from the surroundings, and we removed any unnecessary devices on the tracker that protruded from the plane of array of the modules. The ground surrounding the tracker was a flat gravel surface.
3. **Standard and constant irradiance:** Ideally, if the entire global irradiance of about $1,000 \text{ W/m}^2$ is made up of direct irradiance, then AOI measurements on PV modules become very simple. However, even on very clear days, there is always some diffuse light. Clouds will further increase the ratio of diffuse to direct irradiance. This ratio plays a prominent role in measurement accuracy, especially at higher AOI. Therefore, all the tests were performed under clear sky conditions when the ratio of direct normal irradiance (measured by the normal incidence pyrheliometer) to global normal irradiance (measured by the pyranometer) was higher than 0.85.
4. **Standard and constant spectrum:** Ideally, the test should be performed in a short period of time near solar noon to minimize the influence of spectral variation during the test period. Due to the physical limitation of the tracker, we performed this test around 2:30 pm in order to use the full range of the tracker. However, we

did the test quickly (in about 10 minutes) in order to maintain a constant spectrum throughout the experiment. We changed the AOI by rotating the tracker in azimuth and elevation from west to east up to angles close to 90° (the data obtained in the opposite direction, east to west, is presented in [Appendix F](#)).

5. **Standard and constant temperature:** Ideally, the measurements should be done at a constant module temperature. However, when AOI is changed, the module temperature cannot be kept constant due to varying irradiance level on the module surface. We measured the temperature of each module, under a very low wind speed condition, by attaching a thermocouple to the center of the backsheet and recording the temperature throughout the experiment. Using the measured temperature coefficient for current of each module, we corrected the I_{sc} values to 25°C to eliminate the influence of varying temperature during the test period.
6. **Maximum number of data points:** A higher number of data points will improve the confidence level in the accuracy of measurements. The minimum time interval that the data logger could collect data was 30 seconds. To obtain enough data points, with nearly constant irradiance and AM conditions, we moved the tracker 5° every 30 seconds up to AOI close to 85° (or as far as the tracker would allow). This allowed for a minimum of 18 data points to generate the I_{sc} versus AOI plots (the actual number of data points collected was 21 because we rotated the tracker more slowly at higher AOI to obtain more data points).

RESULTS AND DISCUSSION

Relative I_{sc} With Diffuse Component and Cosine Effects

We selected the first set of data when the ratio of direct normal irradiance (G_{dni}) to total plane of irradiance (G_{tpoa}) was 87%. During this experiment, we measured the I_{sc} data of each module and collected the I_{sc} data for each AOI. Figure 5 shows the I_{sc} data relative to the I_{sc} data obtained at zero AOI. This plot indicates that the data is amazingly identical for all the modules with glass superstrate regardless of the test technology (mono-Si, poly-Si, a-Si, CdTe, or CIGS). It is important to note that both optical and cosine effects of both the direct component and the diffuse component of the incident irradiance influence relative I_{sc} data. In order to obtain the true I_{sc} value (relative light transmission or relative optical response) free from the influence of the diffuse light component and the cosine effect, the I_{sc} data shown in Figure 5 needs to be corrected.

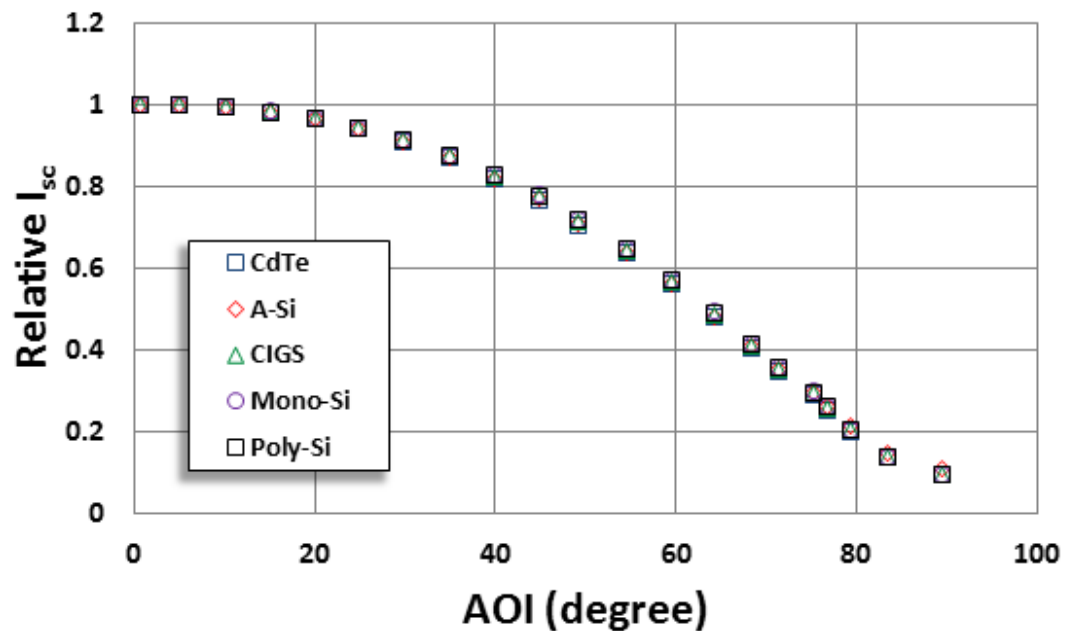


Figure 5. Relative I_{sc} with diffuse component and cosine effects.

Relative I_{sc} Without Diffuse Component and Cosine Effects

According to the requirements of the standard, the diffuse component of the incident light should not exceed 10% of the total irradiance during the experiment. If it does, then the data should be corrected to eliminate the influence of the diffuse component. This correction can be made using the reference cell method or the pyranometer/pyrheliometer method described in the standard and delineated in the [Outdoor Measurement Procedure of IEC 61853-2 Standard](#) section of this report.

To make the correction using the reference cell method, follow the procedure delineated in the standard: “If the diffuse component exceeds 10%, it can be subtracted after measuring the angular response with blocked direct light component or the diffuse component can be blocked to below 10% by reducing the field of view of the diffuse component, for example by collimating the incident light reaching the test module.” The I_{sc} data obtained with this correction method is now influenced only by the direct irradiance without any influence from diffuse irradiance, because the I_{sc} contribution from diffuse irradiance is subtracted from the I_{sc} value obtained with total irradiance.

This I_{sc} data, referred to as $I_{sc}(\theta)$, can then be directly used in equation 3 of this report (or equation 2 of the standard) to obtain the relative light transmission (or relative optical response) data, which is the true corrected data after eliminating the cosine and diffuse component effects.

For the correction using the pyranometer/pyheliometer method, we evaluated the IEC (IEC, 2012) and Sandia (King, Kratochvil, & Boyson, 1997) procedures/models. The IEC procedure/model is briefly described in the [Outdoor Measurement Procedure of IEC 61853-2 Standard](#) section of this report. The Sandia procedure/model involves equations 4 and 5 and the details of this procedure are provided in Appendix A (King, 2012). The relative optical response, $f_2(AOI)$, is given as:

$$f_2(AOI) = \frac{\left[E_0 \left(\frac{I_{sc}}{(1 + \alpha_{isc}(T_c - 25)) \cdot I_{scr}} \right) - \left((E_{poa} - E_{dni} \cdot \cos(AOI)) \right) \right]}{[E_{dni} \cdot \cos(AOI)]} \quad (4)$$

$$I_{scr} = (I_{sc} * E_o) / \{ E_{poa} * (1 + \alpha_{isc} (T_c - 25)) \} \quad (5)$$

Where:

- E_{dni} = Direct normal solar irradiance (W/m^2)
- E_{poa} = Global solar irradiance on the plane-of-array (module) (W/m^2)
- E_o = Reference global solar irradiance, typically $1000 W/m^2$
- AOI = Angle between solar beam and module normal vector (degrees)
- T_c = Measured module temperature ($^{\circ}C$)
- α_{isc} = Short circuit current temperature coefficient ($1/^{\circ}C$)
- I_{scr} = Module short circuit current at STC (A)
- I_{sc} = Measured short circuit current (A)

The plots obtained using the IEC procedure (equations 1, 2, and 3) and the Sandia procedure (equations 4 and 5) are provided in Figures 6 and 7, respectively. Both the IEC model and the Sandia model yield practically the same result. As shown in Figure 8, the modeled data can be slightly influenced at higher AOI values ($> 60^{\circ}$) by the pyranometer type (Eppley or Kipp & Zonen) probably due to the AOI sensitivity of the calibration factors of the pyranometers above 60° .

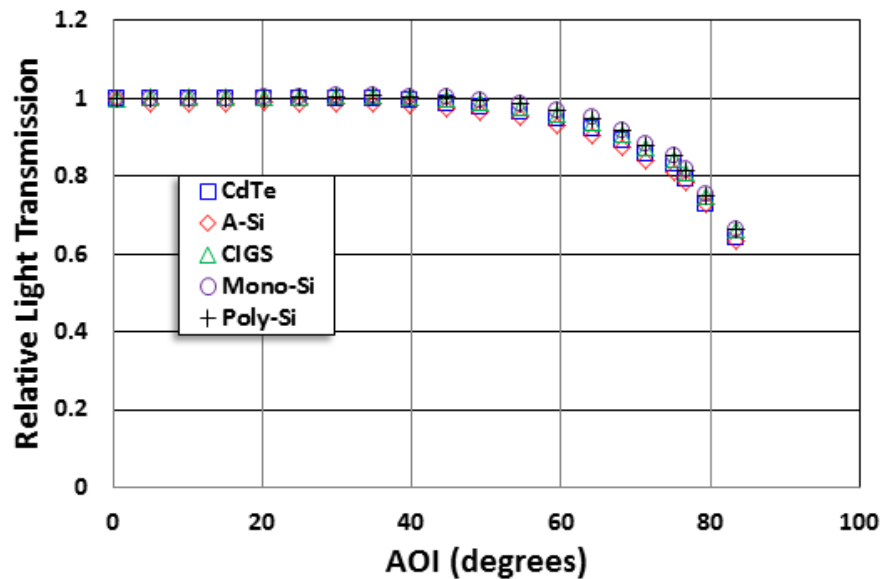


Figure 6. Relative I_{sc} without diffuse component and cosine effects—IEC method.

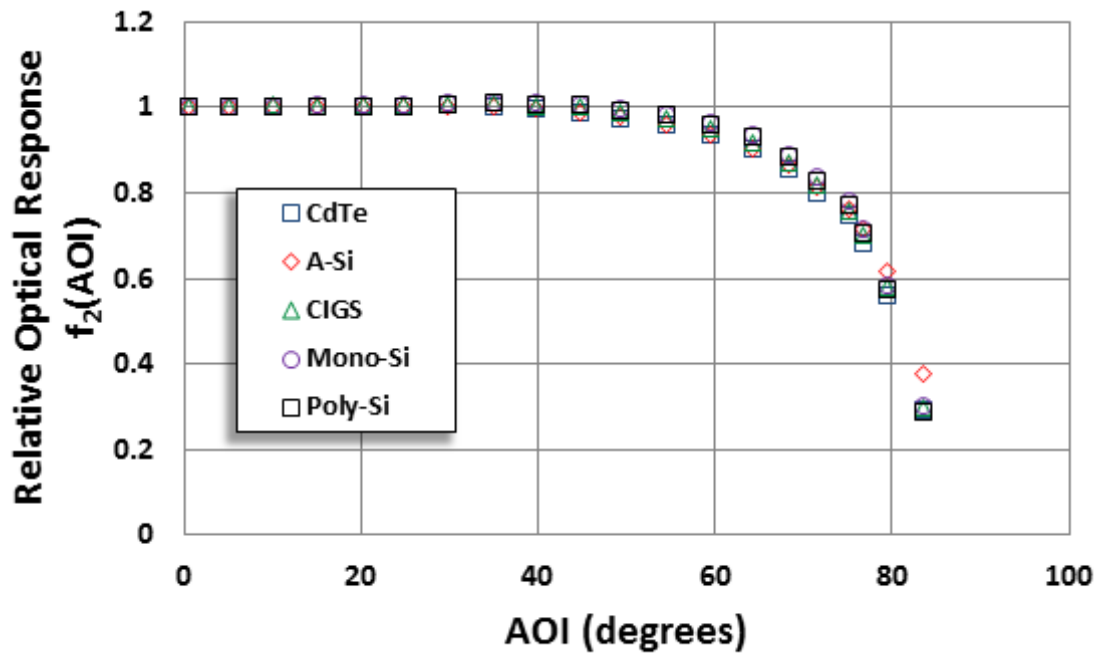


Figure 7. Relative I_{sc} without diffuse component and cosine effects—Sandia method.

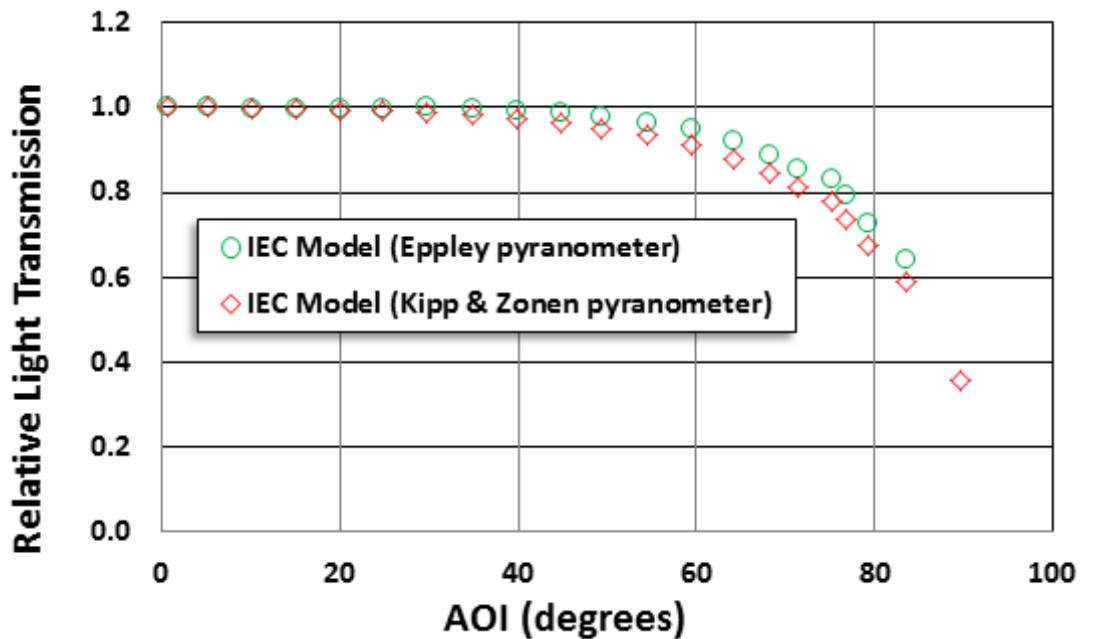


Figure 8. Comparison between Eppley and Kipp & Zonen pyranometers—CdTe Module.

Both the reference cell and pyranometer/pyrheliometer methods have advantages and disadvantages. The reference cell method reduces or eliminates the spectral mismatch error (if the test duration is long) between the reference cell and test module when matched reference cell technology is used, but it requires additional module measurements with blocked or collimated lights. The pyranometer/pyrheliometer method eliminates the additional module measurements, but there could be a spectral mismatch error between the test module, pyranometer, and pyrheliometer if the AM is much higher than 1.5. If the experiment duration is very short, this error can be nearly eliminated and can be considered a second order issue with little or no influence on the final results.

Comparison Between the Models

Based on the $f_2(\text{AOI})$ data obtained for various PV module technologies with glass superstrate, Sandia developed a “generic” polynomial model as shown in equation 6 (see Appendix A for details).

$$f_2(\text{AOI}) = 1 - 2.4377\text{E-}3(\text{AOI}) + 3.1032\text{E-}4(\text{AOI})^2 - 1.2458\text{E-}5(\text{AOI})^3 + 2.1122\text{E-}7(\text{AOI})^4 - 1.3593\text{E-}9(\text{AOI})^5 \quad (6)$$

Several AOI models have been developed and reported for the glass/air interface (Martin & Ruiz, 2005) (Soto, Klein, & Beckman, 2006) (Sjerps-Koomen, Alsema, & Turkenburg, 1997). We compared the data obtained using the Sandia model and the IEC model for the CdTe module (glass superstrate) with the “generic” polynomial model of Sandia and glass/air AOI model of Martin and Ruiz (Martin & Ruiz, 2005). They all have an excellent match with each other, confirming that the relative optical response of all the glass superstrate modules is almost exclusively dictated by the glass/air interface. The draft standard states: “For modules with a flat uncoated front glass plate made of standard solar glass, the relative light transmission into the module is primarily influenced by the first glass-air interface. In this case, the test does not need to be performed, rather, the data of a flat glass air interface can be used.” The experimental and modeled data presented in this report fully validate this statement.

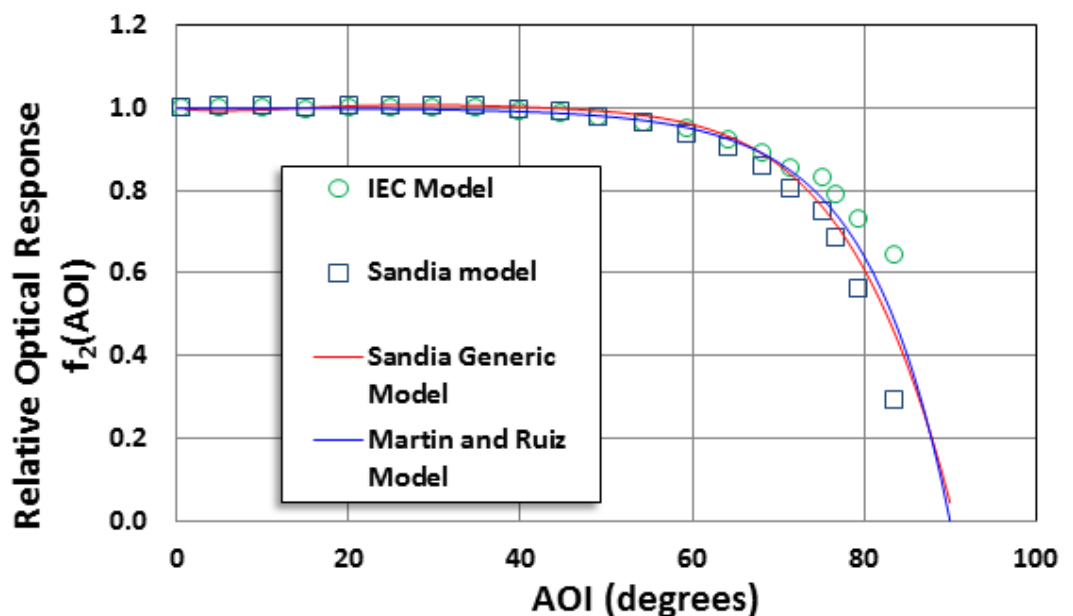


Figure 9. Comparison between various models developed by different institutions.

For a more accurate and repeatable process to test non-glass (including antireflective coated glass) or non-planar (non-flat) glass superstrate modules, follow the reference module (with flat glass superstrate and matched cell technology) approach suggested by Sandia National Laboratories (see Appendix A). Because all the models for the flat glass-air interface are leading to identical results, the reference module (flat glass with matched cell technology) and test module may be tested side-by-side to quickly identify and eliminate the experimental and data processing errors, if any.

UNCERTAINTY ANALYSIS

We took great care during the test setup and procedure to ensure accuracy, but minor errors are inevitable. For equations 4 and 5, each uncertainty contributor was taken into account and the magnitude of the associated uncertainty was assigned based on the calibration report or manufacturer specifications. Table 1 lists the uncertainty contributors and their uncertainties.

Table 1
Uncertainty of Various Uncertainty Contributors in Equations 4 and 5

Uncertainty Contributor (U_i)	Uncertainty
I_{sc} (U_{isc})	1.00%
Global Irradiance (U_{epoa})	1.40%
Temperature Coefficient (U_{alpha})	0.01%
Module Temperature (U_t)	0.75%
Direct Irradiance (U_{dni})	1.10%
Angle of Incidence (U_{AOI})	1.00%

The combined standard uncertainty for f_2 (AOI) was quantified by taking the square root of the sum of the squares of the uncertainty estimates multiplied by the squares of their corresponding sensitivity coefficients. The sensitivity coefficients are determined by taking the derivative of the f_2 (AOI) equation with respect to the uncertainty contributor.

$$u_c = \sqrt{\sum_i c_i^2 u_i^2} \quad (7)$$

The resulting uncertainties are presented as error bars in Figure 10 for each module. As calculated from the equation, the combined uncertainty for f_2 (AOI) increases with increasing AOI. This can be attributed to a greater dependence on the accuracy of the pyranometer at higher AOI. For this experiment, a single sensitivity/calibration factor for the pyranometers was used for all AOI values. However, as discussed previously, the sensitivity factor is expected to vary slightly with an increase in AOI beyond 60°. Therefore, the accuracy of the pyranometer decreases with increasing AOI and the uncertainty of f_2 (AOI) is expected to increase.

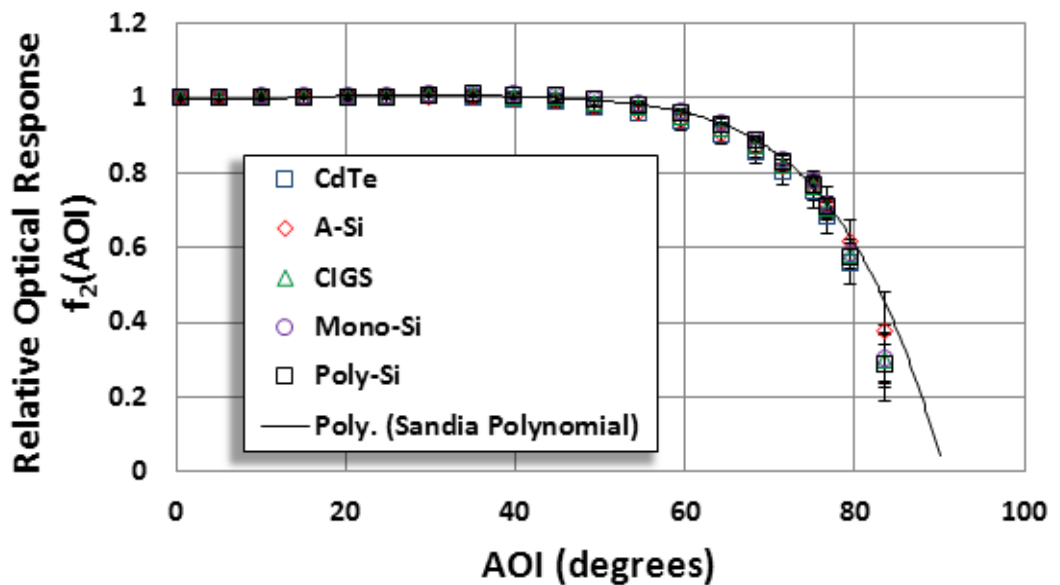


Figure 10. Relative optical response with error bars for all five module technologies.

CONCLUSIONS

During this project, we successfully tested and validated the draft IEC 61853-2 standard procedure for the measurement of incident angle effects on PV modules using an outdoor test method on five PV modules of different technologies.

Our major conclusions include:

- The results show nearly identical relative light transmission plots for all five test modules with glass superstrate regardless of the type of PV cell technology (mono-Si, poly-Si, a-Si, CdTe, or CIGS). This indicates that the reflective losses are governed almost exclusively by the air-glass interface of the PV module.
- The relative light transmission plots obtained using the IEC 61853-2 model were in good agreement with the plots obtained using the theoretical air-glass interface models and the empirical model developed by Sandia National Laboratories for glass superstrate PV modules.
- The standard states that “for the flat glass superstrate modules, the AOI test does not need to be performed, rather, the data of a flat glass air interface can be used.” The results of this study validate this statement.
- Obtaining accurate results required careful experimental setup and rigorous test procedures.
- For a more accurate and repeatable process to test non-glass or non-planar (non-flat) glass superstrate modules, the reference module (with flat glass superstrate and matched cell technology) approach suggested by Sandia National Laboratories (Appendix A) may be followed. The reference module and test module may be tested side-by-side to quickly identify and eliminate the experimental and data processing issues, if any.

ACRONYMS

AM	air mass
AOI	angle of incidence
a-Si	amorphous silicon
ASU-PRL	Arizona State University Photovoltaic Reliability Laboratory
CdTe	cadmium telluride
CIGS	copper indium gallium selenide
cos	cosine
DAS	data acquisition system
DC	direct current
E_{dni}	direct normal solar irradiance (W/m^2)
E_{poa}	global solar irradiance in the plane-of-array (module) (W/m^2)
EVA	ethylene vinyl acetate
IEC	International Electrotechnical Commission
I_{sc}	short circuit current
I-V	current-voltage
mono-Si	monocrystalline silicon
poly-Si	polycrystalline silicon
PV	photovoltaic
Solar ABCs	Solar America Board for Codes and Standards
STC	standard test conditions

REFERENCES

International Electrotechnical Commission (IEC) 61853-2 (Draft). (May 2012). Photovoltaic (PV) module performance testing and energy rating—Part 2: Spectral response, incidence angle and module operating temperature measurements.

King, D.L., Kratochvil, J. A., & Boyson, W.E. (1997). *Measuring solar spectral and angle-of-incidence effects on photovoltaic modules and solar irradiance sensors*. Paper presented at IEEE Photovoltaic Specialists Conference, Anaheim, California.

King, D.L. (June 2012). Measuring angle of incidence (AOI) influence on PV module performance. Private communication (this document is reproduced in Appendix A of this report).

Martin, N. & Ruiz, J.M. (2005). Annual angular reflection losses in PV modules. *Progress in Photovoltaics*. 13. 75–84.

Sjerps-Koomen, E.A., Alsema, E.A., & Turkenburg, W.C. (1997). A simple model for PV module reflection losses under field conditions. *Solar Energy*. 57. 421-432.

Soto, W.D., Klein, S. A., & Beckman, W.A. (2006). Improvement and validation of a model for photovoltaic array performance. *Solar Energy*. 80. 78–88.

SCOPE OF APPENDICES

Appendix A: Sandia Procedure to Determine Relative Optical Response

The Sandia procedure to measure relative optical response has already been published (King, Kratochvil, & Boyson, 1997). An extended and detailed version of this procedure was recently documented in a private communication, and this document is reproduced in Appendix A.

Appendix B: Crosschecking of AOI Device Using a Manual Method

We directly measured the AOI data provided in this report using a 3DM-GX3-25 sensor from MicroStrain. In order to crosscheck that these measured data are accurate, we also manually determined the AOI data, and Appendix B discusses this process. We found that the AOI data obtained by the sensor and manual methods matched.

Appendix C: Lessons Learned 1: Round 1 Measurements Using a Multi-Curve Tracer

During the first round of measurements, we used a multi-curve tracer to obtain the entire current-voltage (I-V) curve including the short circuit current data required for the AOI experiment. We discuss the lessons learned during the first round of measurements in Appendix C. (Note that during the third and final round of measurements, we used calibrated transducers and a data logger with a multiplexer to gather the data that we used in the body of this report.)

Appendix D: Lessons Learned 2: Round 2 Measurements Using Transducers and Data Logger

During the second round of measurements, the transducers and data logger we used were not calibrated, so we could not do an uncertainty analysis. We present the lessons learned during the second round of measurements in Appendix D. (Note that during the third and final round of measurements, we used calibrated transducers and a data logger with a multiplexer to gather the data that we used in the body of this report.)

Appendix E: Inter-Comparison and Crosschecking of Pyranometers

Because the accuracy of the data obtained from the pyranometer is extremely important in these relative light transmission experiments, we decided to compare and crosscheck the data using two calibrated pyranometers from two different manufacturers. Appendix E provides inter-comparison results obtained with Eppley and Kipp & Zonen pyranometers.

Appendix F: Measurement of $f_2(\text{AOI})$ Versus AOI in the Opposite Direction

The standard states: “For devices with rotational symmetry of the reflectivity with respect to the module normal, do a minimum of 9 different angles to span the angles from 0 to 80° for one direction and assume the reflectivity to be identical for the second orthogonal direction. For rotationally asymmetrical devices, the full measurement series needs to be carried out for two orthogonal directions across the module plane.” In order to determine whether the test modules have any asymmetric behavior for the reflectivity, we carried out these measurements for both directions and we present the results of these measurements in Appendix F.

APPENDIX A: SANDIA PROCEDURE TO DETERMINE RELATIVE OPTICAL RESPONSE, $f_2(\text{AOI})$

Measuring Angle of Incidence (AOI) Influence on PV Module Performance

Private Communication with David L. King (June 2012)

There are two AOI influences that need to be considered—“mechanical” and “optical.” The mechanical influence really doesn’t have anything to do with the module itself, but rather its orientation relative to the incident sunlight, often called the “cosine effect.” The beam solar irradiance incident on the module is reduced by $\cos(\text{AOI})$.

The optical effect is due to the surface characteristics of the module, which can be highly planar (float glass), dimpled (rolled glass), coated with antireflective (AR) coatings, heavily textured for light gathering at large AOI, or specifically patterned for optical concentration purposes. The primary influence on the optical effect is increasing reflectance loss as AOI increases. Both of these AOI influences apply primarily to the beam or direct component of sunlight, rather than the diffuse component of sunlight.

The Sandia module performance model attempts to account for both these influences using an expanded expression for the solar irradiance, called the effective solar irradiance (E_e), which in turn determines the module’s short circuit current (I_{sc}). Equation (A1) gives the Sandia expression for E_e , and Equation (A2) gives the resulting equation for I_{sc} . The intent of this document is to provide a discussion of the procedures that can be used to empirically measure the optical effect, $f_2(\text{AOI})$.

$$E_e = [E_{dni} * \cos(\text{AOI}) * f_2(\text{AOI}) + f_d * (E_{poa} - E_{dni} * \cos(\text{AOI}))] / E_o \quad (\text{A1})$$

$$I_{sc} = I_{sco} * [1 + \alpha_{isc} * (T_c - 25)] * f_1(\text{AM}_a) * E_e \quad (\text{A2})$$

Where:

E_e = Solar irradiance actually captured and used by module (effective irradiance)

E_{dni} = Direct normal solar irradiance (W/m^2)

E_{poa} = Global solar irradiance in the plane-of-array (module) (W/m^2)

E_o = Reference global solar irradiance, typically $1000 \text{ W}/\text{m}^2$

f_d = Fraction of diffuse irradiance used by module, typically assumed = 1

AOI = Angle between solar beam and module normal vector (degrees)

T_c = Measured module (cell) temperature ($^{\circ}\text{C}$)

α_{isc} = Short circuit current temperature coefficient ($1/^{\circ}\text{C}$)

$f_1(\text{AM}_a)$ = Empirical relationship for solar spectral influence on I_{sc} versus air mass

I_{sco} = Module short circuit current at standard test conditions (STC) (A)

I_{sc} = Measured short circuit current (A)

Direct Measurement of $f_2(\text{AOI})$

The direct procedure for measuring $f_2(\text{AOI})$ involves measuring module I_{sc} as the module is moved in angular increments using a solar tracker through a wide range of AOI conditions, 0° to 90° . The challenge is to conduct the test in a way that either minimizes or compensates for all the factors in Equations (A1) and (A2) that influence the measured I_{sc} values. The following list identifies desirable conditions and approaches, depending on the capabilities of the test equipment available:

- Conduct test during clear sky conditions when the direct normal irradiance is the dominant component; for example, when the ratio of direct normal divided by global normal irradiance is greater than about 0.85. This reduces the influence of diffuse irradiance on the determination of $f_2(\text{AOI})$.

- Conducting the test near solar noon also has a couple advantages—variation in the solar spectrum during the test is minimized, and the full range for AOI can typically be achieved by changing only the elevation angle of a two-axis solar tracker.
- Measure I_{sc} , E_{dni} , E_{poa} , and T_c associated with each AOI increment. E_{dni} should be measured with a thermopile pyrheliometer, and E_{poa} should ideally be measured using a thermopile pyranometer that has been calibrated as a function of AOI.
- Module temperature will vary during the test, so measured temperature should be used to translate measured I_{sc} values to a common temperature; for example, 25°C.
- If possible, record data over the full range of AOI as rapidly as possible, so that solar spectral variation can be ignored. A less than 30-minute test period is desirable. If the test period must be longer, then a spectral correction to measured I_{sc} can be done using a previously determined $f_1(AM_a)$ relationship.

The Sandia model Equations (A1) and (A2) can be solved to provide an equation for the angle-of-incidence relationship, $f_2(AOI)$, as a function of the measured variables, Equation (A3).

$$f_2(AOI) = \{ [I_{sc} * E_o / (I_{sco} * f_1(AM_a) * (1 + \alpha_{isc}(T_c - 25)))] - f_d * (E_{poa} - E_{dni} * \cos(AOI)) \} / (E_{dni} * \cos(AOI)) \quad (A3)$$

In order to simplify, recognize that by definition $f_2(AOI) = 1$ when $AOI = 0^\circ$. Therefore, Equation (A3) can be solved for the I_{sco} value at the start and end of the outdoor test period when $AOI = 0^\circ$. The value solved for is not exactly I_{sco} at STC because the air mass value may not be exactly $AM_a = 1.5$ at the time of day when the $AOI = 0^\circ$ conditions were achieved. This calculated value is only intended to provide a reference value for I_{sc} in order to normalize $f_2(AOI) = 1$ when $AOI = 0^\circ$, so to avoid confusion call the calculated value I_{scr} .

$$I_{scr} = I_{sc} * E_o / \{ f_1(AM_a) * (1 + \alpha_{isc}(T_c - 25)) * (E_{dni} + f_d * (E_{poa} - E_{dni})) \} \quad (A4)$$

After determining the value for I_{scr} using the average value for several measurements when $AOI = 0^\circ$, the measured values for $f_2(AOI)$ can be determined using Equation (A3) by substituting the I_{scr} value for I_{sco} .

Further simplification in the determination of $f_2(AOI)$ can be made for conventional flat-plate modules, depending on the test procedure and assumptions made. If data for the full range of AOI is recorded in a relatively short period of time, then the influence of varying solar spectrum is likely to be negligible. In addition, for conventional flat-plate modules the assumption is usually made that they capture both diffuse and direct irradiance; therefore $f_d = 1$. Under these simplified conditions, Equations (A3) and (A4) can be rewritten as Equations (A5) and (A6).

$$I_{scr} = (I_{sc} * E_o) / \{ E_{poa} * (1 + \alpha_{isc}(T_c - 25)) \} \quad (A5)$$

$$f_2(AOI) = [E_o * (I_{sc} / (1 + \alpha_{isc}(T_c - 25))) / I_{scr} - (E_{poa} - E_{dni} * \cos(AOI))] / (E_{dni} * \cos(AOI)) \quad (A6)$$

For conventional flat-plate glass modules, this procedure should result in empirical $f_2(AOI)$ relationships similar to those shown in Figure A1. As previously mentioned, AR-coated glass or heavily textured glass will provide different results. For the simple case with a planar glass surface, Snell's and Bouguer's optic laws along with glass optical properties (index of refraction, extinction coefficient, thickness) can also be used to calculate a theoretical relationship for $f_2(AOI)$ (Soto, Klein, & Beckman, 2006).

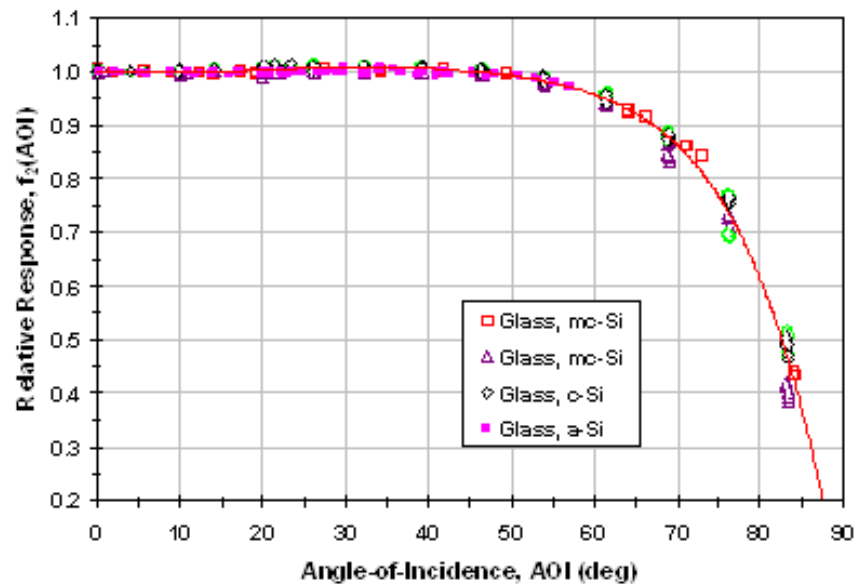


Figure A1. Empirical $f_2(AOI)$ measurements by Sandia National Laboratories for conventional flat-plate modules with planar glass front surfaces.

Although polynomial fits to measured data can be problematic, ten years ago when the procedure was developed and the Sandia module database initiated, a fifth order fit was used to represent the measured data. There are probably better ways to represent the data, but at this point the Sandia module database has gained enough inertia that it would be difficult to change the model coefficients used to match the measured data. The “generic” polynomial used for the majority of typical glass-surface modules is given below.

$$f_2(AOI) = 1 - 2.4377E-3(AOI) + 3.1032E-4(AOI)^2 - 1.2458E-5(AOI)^3 + 2.1122E-7(AOI)^4 - 1.3593E-9(AOI)^5$$

Relative (Comparison) Measurements for $f_2(AOI)$

Although not presented in this document, an alternative test procedure providing simultaneous measurements of the I_{sc} of a test module and a reference module may possibly provide a more accurate and repeatable process. The reference module is assumed to have “known $f_2(AOI)$ ” characteristics. The reference device could be a module or an individual reference cell, ideally with matching cell technology to provide equivalent solar spectral sensitivity. For a reference device with ideally planar glass surface, the “known $f_2(AOI)$ ” could be derived from optical laws, perhaps providing a more fundamental basis for the outdoor test procedure.

REFERENCE

Soto, W.D., Klein, S. A., & Beckman, W.A. (2006). Improvement and validation of a model for photovoltaic array performance. *Solar Energy*. 80. 78–88.

APPENDIX B: CROSSCHECKING OF AOI DEVICE USING A MANUAL METHOD

In this study, the AOI was directly determined using an AOI device purchased from MicroStrain. However, in the absence of this device, the AOI value can also be determined using a manual calculation (equation B1) given by Sandia National Laboratories (King, Kratochvil, & Boyson, 1997).

$$AOI = \cos^{-1}(\cos(T_m) \cos(Z_s) + \sin(T_m) \sin(Z_s) \cos(AZ_s - AZ_m)) \quad (B1)$$

Where:

AOI = solar angle of incidence (degrees)

T_m = tilt angle of module (degrees, 0° is horizontal)

Z_s = zenith angle of the sun (degrees)

AZ_m = azimuth angle of module (0° = North, 90° = East)

AZ_s = azimuth angle of sun (degrees)

As shown in Figure B1 (azimuth rotation) and Figure B2 (elevation rotation) below, the accuracy of the AOI device used in this project was crosschecked with the manual method using Equation (B1) above. These plots confirm that the AOI data obtained using the MicroStrain device was reliable and accurate.

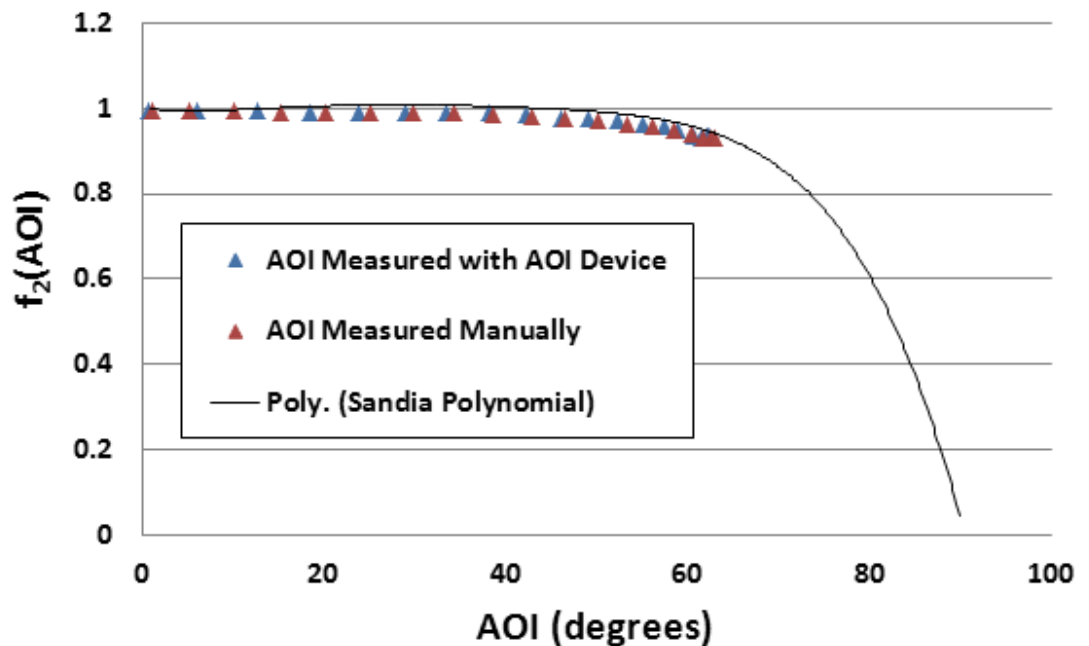


Figure B1. Comparison of relative optical responses obtained using the AOI hardware and AOI calculation for a CdTe module with glass superstrate for azimuth rotation (direct to global ratio was 0.89).

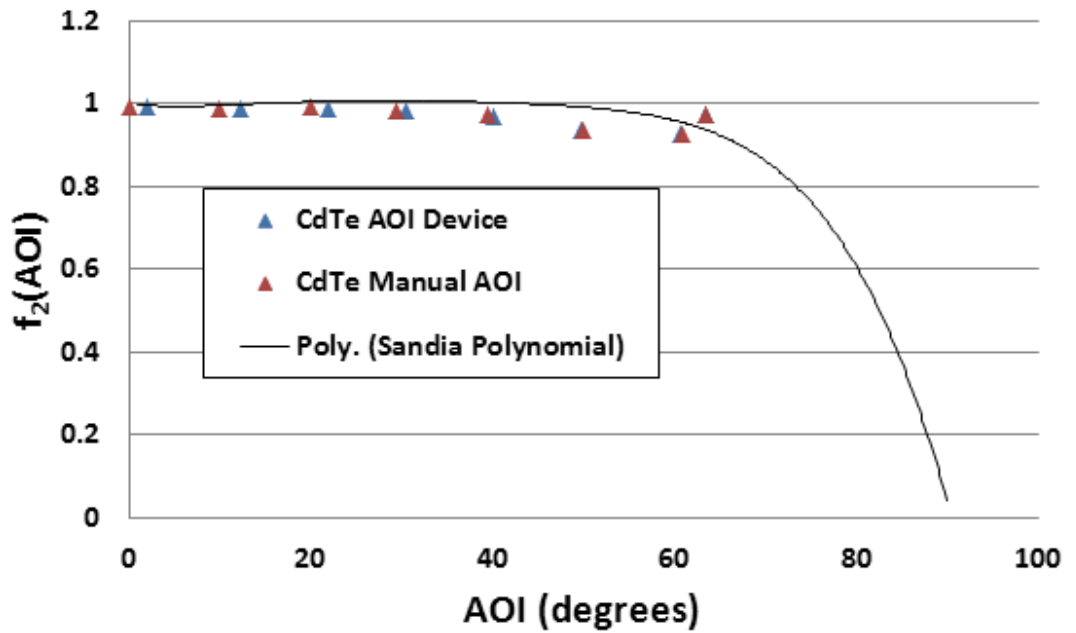


Figure B2. Comparison of relative optical responses obtained using the AOI hardware and AOI calculation for a CdTe module with glass superstrate for elevation rotation (direct to global ratio was 0.89).

For azimuth angle, the tracker was allowed to rotate to its full westward rotation angle and tracked azimuthally to the east. The azimuth angle of the module was manually measured by dividing the diameter of the tracker pole into 360° and fixing a dial to the rotating head of the tracker to indicate its change in angle. Because the azimuthal rotation of the tracker was limited, azimuth verification could only be obtained for AOI up to 63°. For elevation angle, the two-axis tracker was tilted to the maximum horizontal position of 11° (where 0° is horizontal) and tilted downward to a maximum angle of 74.5°. The $f_2(\text{AOI})$ data for elevation angle deviates from the generalized polynomial for higher tilt angles due to the inconsistent reflectance throughout the measurement. When the modules are at 11° tilt (close to horizontal), they “see” only the sky. As they are tilted downward, the ground reflection could interfere with the data accuracy. This phenomenon does not occur for azimuth angles because the modules are essentially seeing the same ratio of sky and ground (they were at 30° tilt angle for the duration of the azimuth rotation).

The purpose of this experiment was to verify that the manual method and AOI device measurements were consistent. Both methods proved to be accurate. The standard deviation between manually calculated AOI and the AOI device measurement for azimuth angle was 1.66°. The standard deviation between manually calculated AOI and AOI device measurement for elevation tilt was 1.08°.

APPENDIX C: LESSONS LEARNED 1: ROUND 1 MEASUREMENTS USING A MULTI-CURVE TRACER

The data presented in the main body of the report (the third and final round) evolved from previous two rounds of data collections and reductions. Improvements to the experimental setup and data processing were made after each round. For the first round of data collection, a DayStar (DS3200) multi-curve tracer was used to measure and record I_{sc} , module temperature, and irradiance sensor readings. The main problems concerning these measurements were:

1. The fastest time the multi-curve tracer could record and store data was one minute intervals. This was due to a software limitation of the multi-curve tracer, not a hardware issue. The multi-curve tracer saves data files onto the hard drive by automatically assigning them a file name based on the time the data was collected. The data file is named only for the hour and minute it is stored (not for the second). The physical capabilities of the tracker allow it to take data for the five modules in ten seconds. However, because the files are automatically assigned a name based on the time they were taken, the minimum time interval the data could be recorded and stored was one minute. For this experiment, the tracker was rotated by 5° AOI every one minute until it reached a maximum of 77° AOI. The experiment was performed in 16 minutes and a total of 16 data points were collected. The 16 data points in 16 minutes are sufficient to comply with the IEC 61853-2 standard, which states “for devices with rotational symmetry of the reflectivity with respect to the module normal, do a minimum of 9 different angles to span the angles from 0 to 80° for one direction.” To confidently validate this statement, however, more data points were needed. Because data should be recorded as quickly as possible to reduce the spectral change during the experiment, round 2 was to be carried out using equipment that could measure and record data in less than one minute intervals.
2. The irradiance sensors used for measuring global irradiance in the plane of array (pyranometers) and direct normal irradiance (pyrheliometer) had not been calibrated, and therefore the accuracy of the measurements could not be confirmed and the uncertainty could not be calculated.
3. The relative I_{sc} obtained versus AOI plot is shown in Figure C1. Using Sandia’s Equation A6, the relative optical response data— f_2 (AOI) data—was plotted versus AOI as shown in Figure C2. The plotted data (symbols) was then compared to the “generic” polynomial curve (solid line) empirically derived by Sandia National Laboratories. As this figure shows, there is a significant difference between the f_2 (AOI) data calculated using the experimental data and the generic polynomial curve (between 60° and 75°). This difference warranted further investigation, which revealed a human error in constructing the Equation A6 in the Excel spreadsheet. This error was fixed in the final rounds of data processing.

Nevertheless, the multi-curve tracer method, as opposed to the transducer/data logger method, was not continued for the second and third (final) rounds of measurements due to the limitation on the number of data points that could be collected during the short duration of tracker rotation.

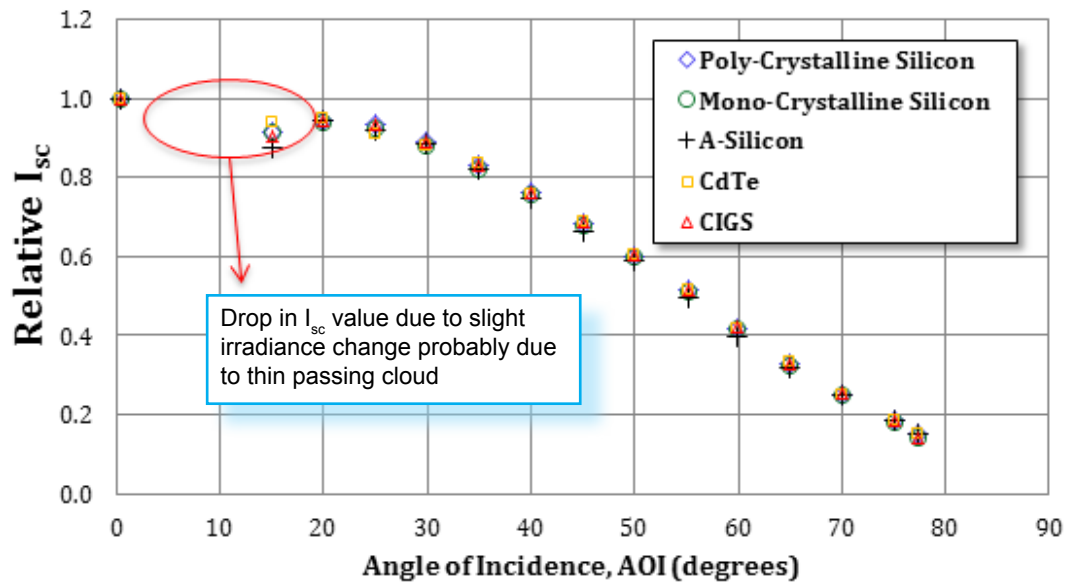


Figure C1. Round 1—Relative I_{sc} versus AOI for five modules (multi-curve tracer method).

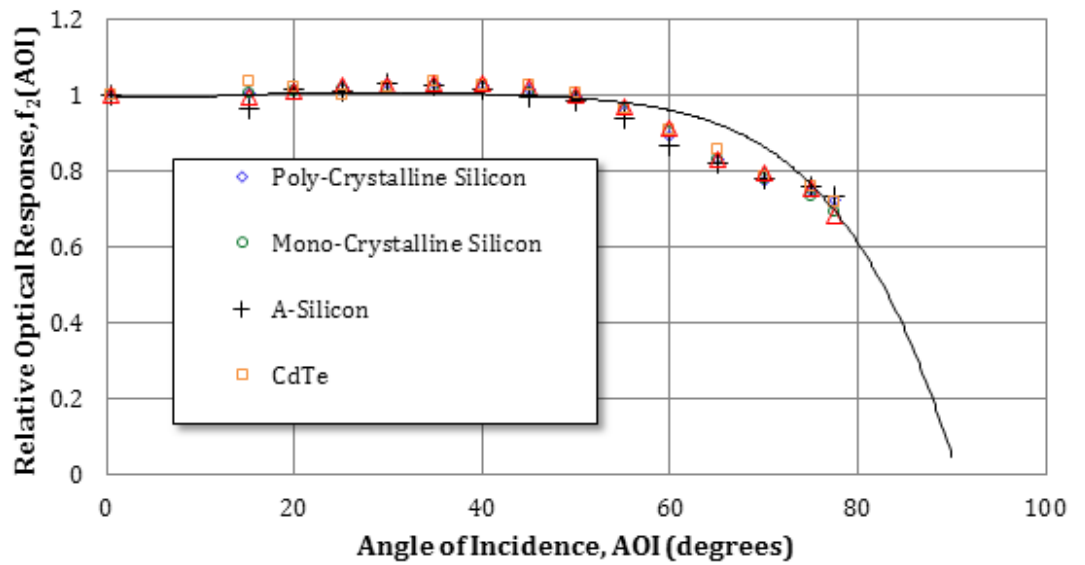


Figure C2. Round 1—Data for five modules where $f_2(AOI)$ was erroneously calculated using Equation A6 (multi-curve tracer method).

APPENDIX D: LESSONS LEARNED 2: ROUND 2 MEASUREMENTS USING TRANSDUCERS AND DATA LOGGER

During round 2, we used CR Magnetics DC current transducers and a Campbell Scientific CR1000 data logger and multiplexer to measure and record I_{sc} , module temperature and reference cell readings. The problems apparent in round 1 were addressed in round 2:

1. The fastest time interval that the multi-curve tracer could measure and store data was one minute. For round 2, the fastest time interval that the data logger and multiplexer could store data was 30 seconds. For round 2, we collected 16 data points during the 9.5-minute experiment.
2. In round 2, we identified and corrected the human error that was present in round 1 when constructing Equation A6 in the Excel spreadsheet. Therefore, all plots presented in round 2 used the correct f_2 (AOI) equation.
3. The reference devices had yet to be calibrated for this experiment. Therefore, uncertainty analysis of f_2 (AOI) could not be calculated.

For round 2 measurements, the relative I_{sc} obtained versus AOI is shown in Figure D1. The plot of f_2 (AOI) versus AOI, which was correctly generated using the Sandia Equation A6, is given in Figure D2.

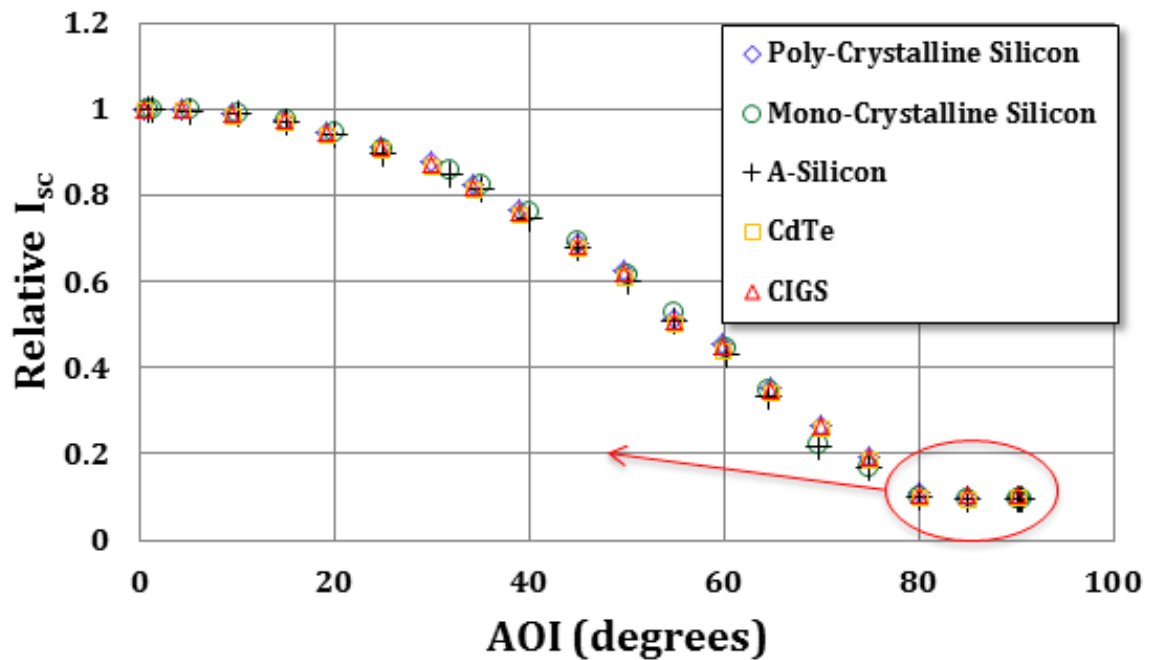


Figure D1. Round 2—Relative short circuit current versus AOI for five modules (data logger method).

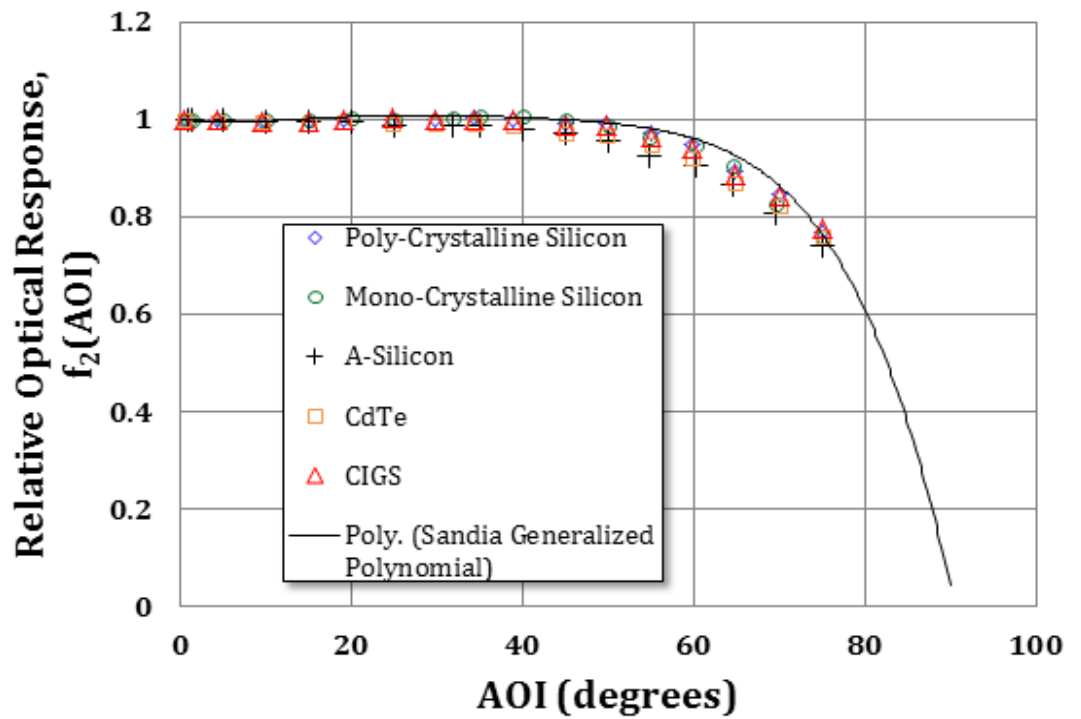


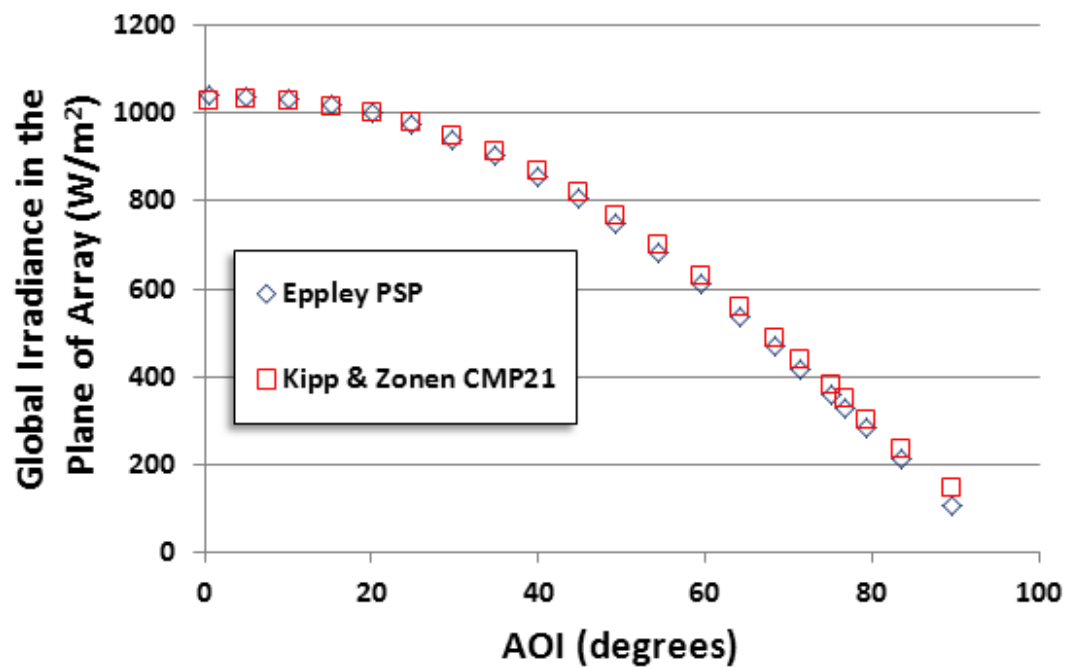
Figure D2. Round 2—Data for five modules where $f_2(\text{AOI})$ was *correctly* calculated using Equation A6 (data logger method).

APPENDIX E:

INTER-COMPARISON AND CROSSCHECKING OF PYRANOMETERS

For this experiment, we used a calibrated Eppley PSP pyranometer to measure global irradiance in the plane of array and cross referenced it with a Kipp & Zonen CMP21. The f_2 (AOI) calculation proved to be extremely sensitive to the accuracy of the global irradiance measurements. We mounted the pyranometers coplanar to the PV modules and in positions on the tracker so that no shading of the modules or the other reference devices occurred. The E_{poa} measurements for both devices were recorded simultaneously by the CR1000 data logger and are shown in Table E1. The AOI experiment was performed on several different days with various ratios of direct normal irradiance to global irradiance (E_{dni}/E_{poa}). For each case, the standard deviation of the pyranometers' measured global irradiance in the plane of array (E_{poa}) increased as AOI increased. Figure E1 gives E_{poa} measured for both pyranometers and their standard deviation as measured for an 87% E_{dni}/E_{poa} ratio.

Figure E1. Global irradiance as measured by the Kipp & Zonen CMP21 and Epply PSP pyranometer for 87% E_{dni}/E_{poa}



E_{dni}/E_{poa} .

Table E1:
Comparison of Kipp & Zonen CMP21 Versus Eppley PSP Measured Global Irradiance
in the Plane of Array for 87% Direct to Global Irradiance Ratio

88% E_{dni} to E_{poa} Ratio			
AOI (degrees)	Kipp & Zonen E_{poa} (W/m ²)	Eppley E_{poa} (W/m ²)	Difference (%)
0.6	1029.3	1038.6	0.9%
5.1	1030.3	1036.4	0.6%
10.1	1026.0	1029.5	0.3%
15.1	1015.2	1018.2	0.3%
20.2	1000.0	1000.0	0.0%
24.9	979.4	976.1	0.3%
29.8	949.1	940.9	0.9%
34.9	913.3	901.5	1.3%
39.9	868.9	854.4	1.7%
44.8	819.7	804.4	1.9%
49.2	764.8	747.8	2.3%
54.5	700.4	681.5	2.8%
59.5	629.9	610.2	3.2%
64.2	559.0	537.4	4.0%
68.3	489.3	468.4	4.5%
71.4	437.2	418.3	4.5%
75.2	381.8	359.9	6.1%
76.8	351.1	329.2	6.7%
79.4	302.6	282.5	7.1%
83.5	233.9	215.8	8.4%
89.6	146.0	109.2	33.7%

The data presented in Table E1 represents the data used in the body of this report. However, we also performed experiments for other days with various direct to global irradiance ratios. Figure E2 gives a comparison of irradiance data for a direct to global irradiance ratio of 81 %. This data also shows a higher standard deviation for higher AOI. For AOI from 0° to 66° the average standard deviation is 4 %, whereas for AOI from 67° to 90° the average standard deviation is 15 %. Figure E3 gives a comparison of irradiance data for an overcast day where the ratio of direct to global irradiance was 2 %. For this data, the standard deviation between the two pyranometers remained approximately constant, but higher, for all AOI.

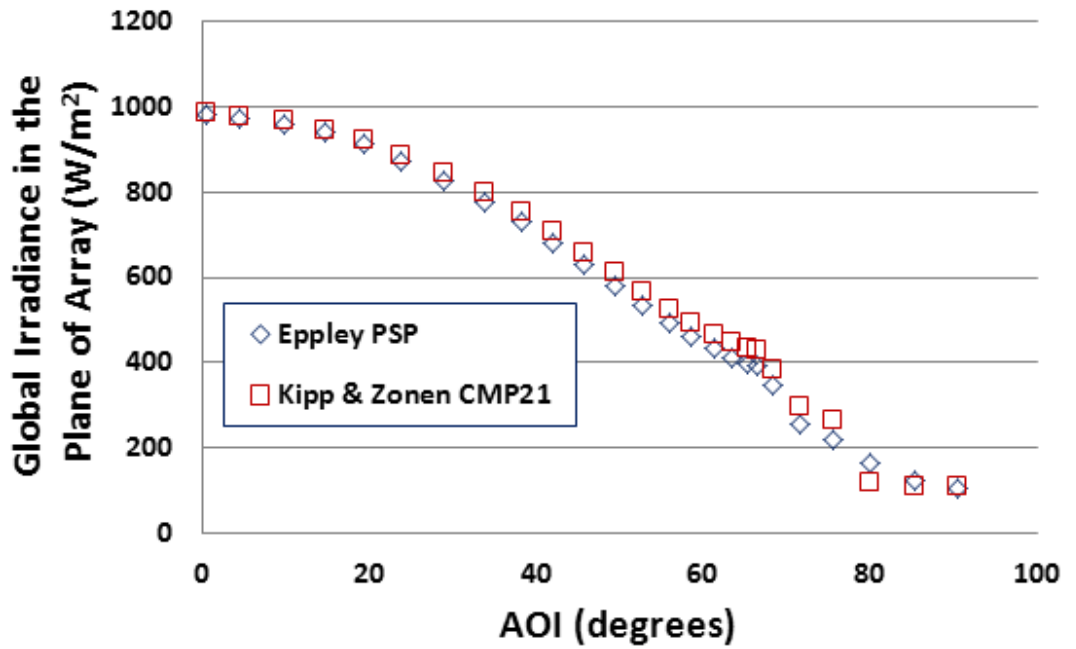


Figure E2. Comparison of Kipp & Zonen CMP21 versus Eppley PSP measured global irradiance in the plane of array for 81 % direct to global irradiance ratio.

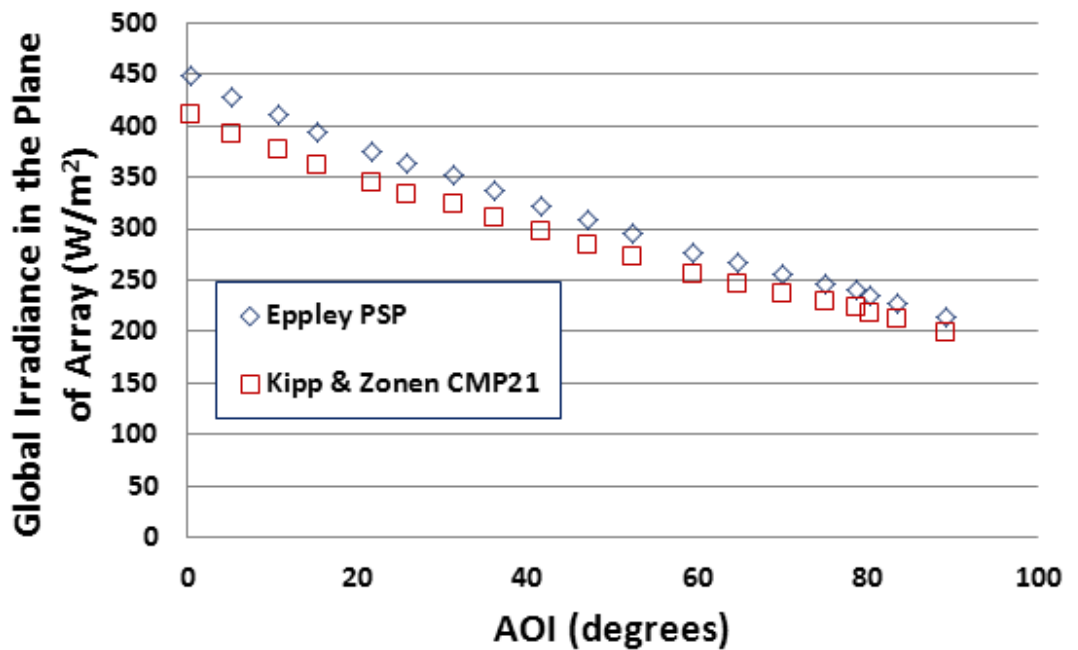


Figure E3. Comparison of Kipp & Zonen CMP21 versus Eppley PSP measured global irradiance in the plane of array for 2% direct to global irradiance ratio.

APPENDIX F: MEASUREMENT OF f_2 (AOI) VERSUS AOI IN THE OPPOSITE DIRECTION

To obtain Figure 7 in the main body of this report, we collected experimental data at 14:37:30 and the tracker was rotated from the west (starting at 0.59° AOI) to the east (ending at 83.50° AOI). This experiment took 10 minutes to complete. To verify the rotational symmetry of the reflectivity with respect to module normal as called for in IEC 61853-2, the data was also collected for the five modules in the opposite direction (east to west). This experiment started at 14:47:30. The tracker was set to automatic mode and allowed to track the opposite direction (from east to west). The data was processed using Sandia Equation A6 and the corresponding graph of f_2 (AOI) is given in Figure F1.

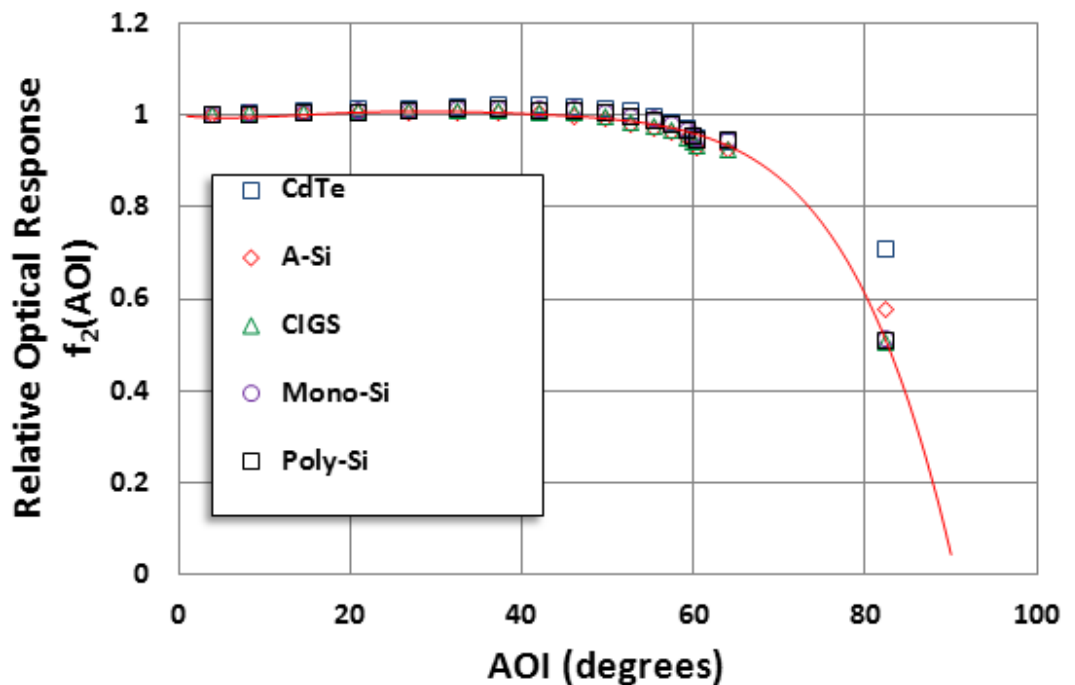


Figure F1. Round 3—Data for five modules where f_2 (AOI) was calculated when the tracker was rotated in the opposite direction (east to west).

Using the automatic function to track in the opposite direction had a few disadvantages. In the manual mode, the tracker was rotated in both azimuth and elevation proportionally. However, when the tracker was set to automatic mode to track back to zero AOI, it first adjusted elevation angle, then tracked back azimuthally. This is not expected to affect the relative optical response of the module, but it does limit the number of data points collected. Tilting the tracker in elevation changes the AOI much more quickly than rotating azimuthally. Because the tracker tilted the modules in elevation for the first 30 seconds, data could only be recorded for AOI of 83° (the starting point taken at 14:37:30) and 63° (the next point taken at 14:38:00). After the tracker had adjusted its elevation angle it began tracking azimuthally, and more data points could be obtained. Figures F2 through F6 give the plots for f_2 (AOI) calculated for each module technology tracking in both directions (east to west and west to east). The data for each technology is consistent for AOI when rotated in both directions from 0 to 63° .

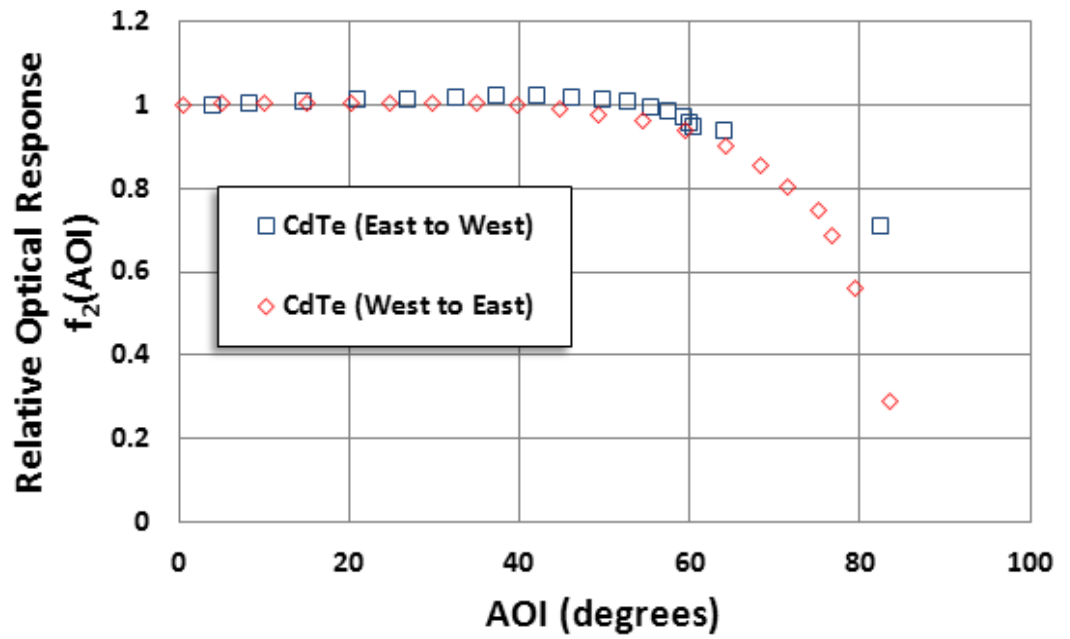


Figure F2. Round 3—Data for $f_2(AOI)$ calculated for CdTe from west to east compared to data when the tracker was rotated in the opposite direction (east to west).

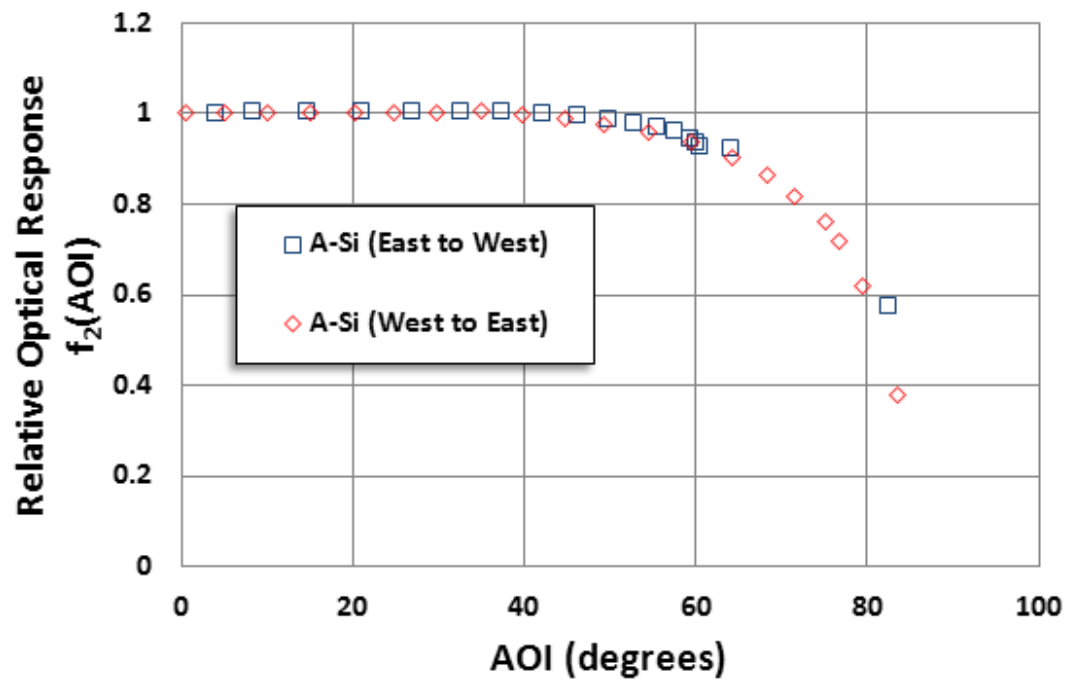


Figure F3. Round 3—Data for $f_2(AOI)$ calculated for a-Si from west to east compared to data when the tracker was rotated in the opposite direction (east to west).

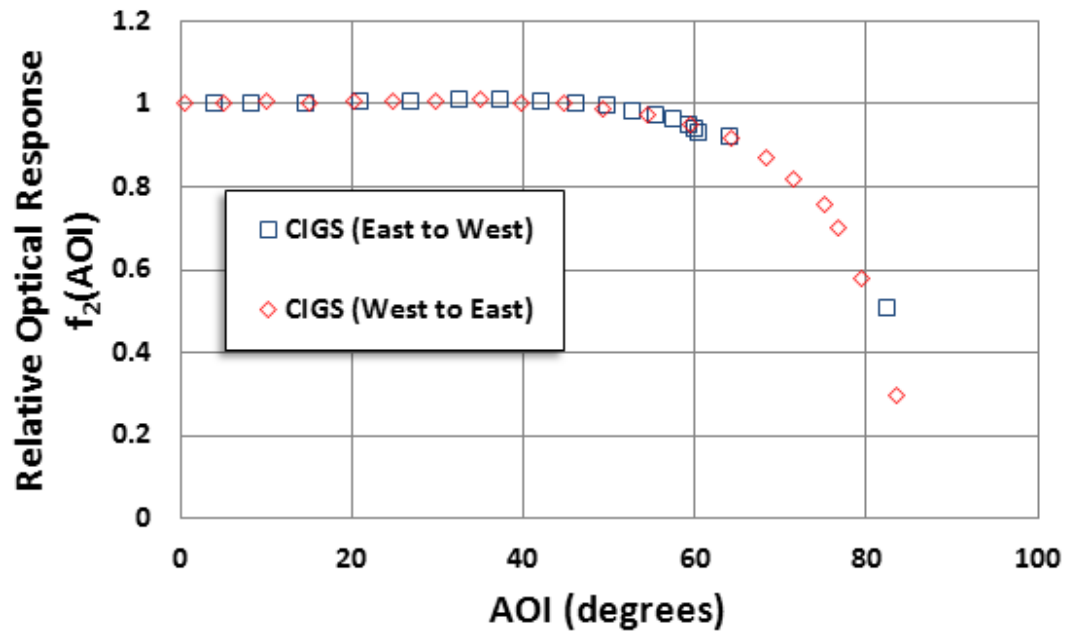


Figure F4. Round 3—Data for $f_2(\text{AOI})$ calculated for CIGS from west to east compared to data when the tracker was rotated in the opposite direction (east to west).

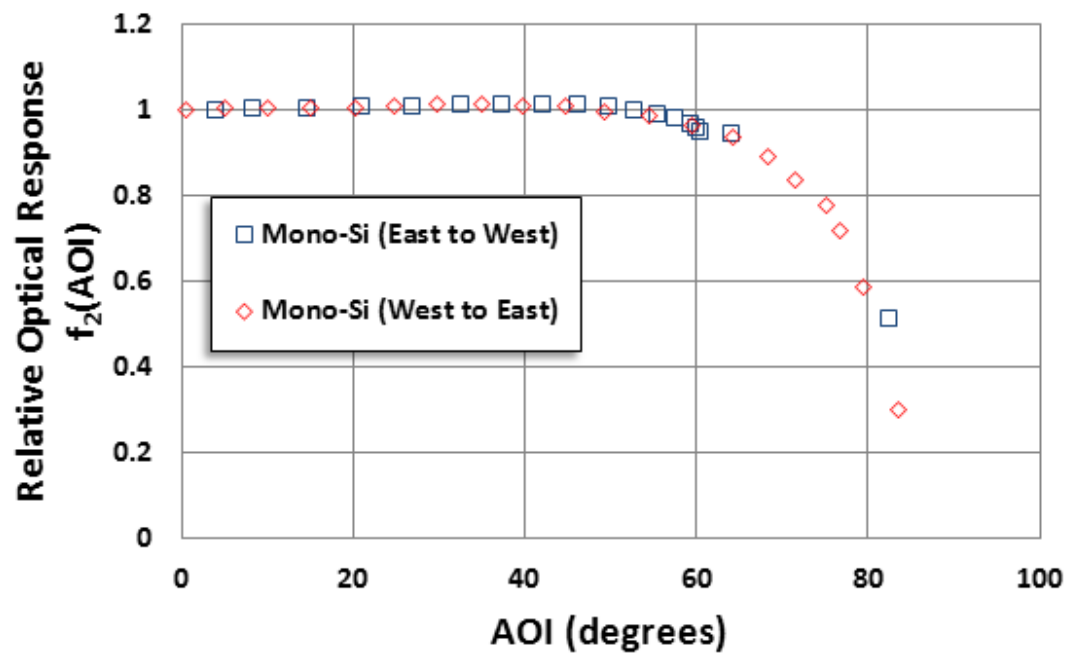


Figure F5. Round 3—Data for $f_2(\text{AOI})$ calculated for mono-Si from west to east compared to data when the tracker was rotated in the opposite direction (east to west).

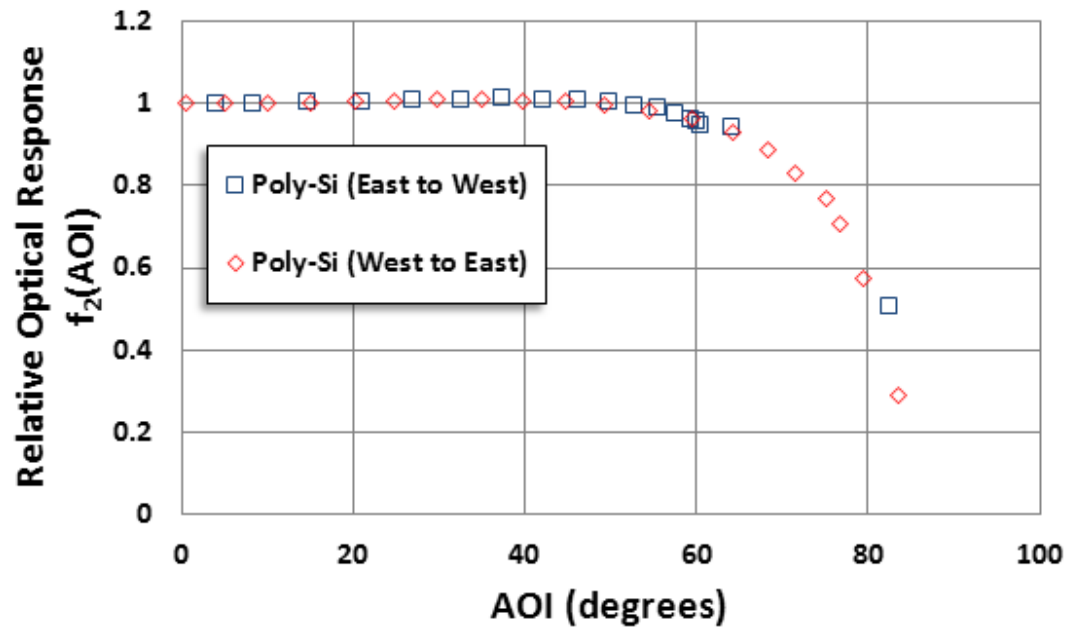


Figure F6. Round 3—Data for $f_2(AOI)$ calculated for poly-Si from west to east compared to data when the tracker was rotated in the opposite direction (east to west).



Solar America Board for Codes and Standards

www.solarabcs.org